**RICE UNIVERSITY**

**Regular Arrays of QDs by Solution Processing**

by

**BRITTANY L. OLIVA**

A THESIS SUBMITTED
IN PARTIAL FULFILLMENT OF THE
REQUIREMENTS FOR THE DEGREE OF
**Master of Science**

APPROVED, THESIS COMMITTEE

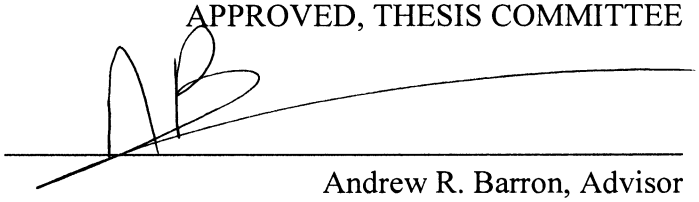

Andrew R. Barron, Advisor
Charles W. Duncan, Jr. – Welch Chair of Chemistry
Professor of Chemistry and Materials Science

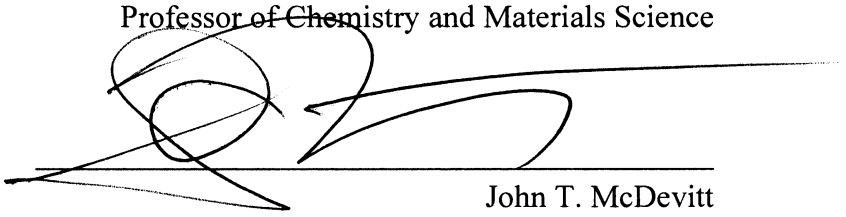

John T. McDevitt
Brown – Wiess Professor of Chemistry and Bioengineeing

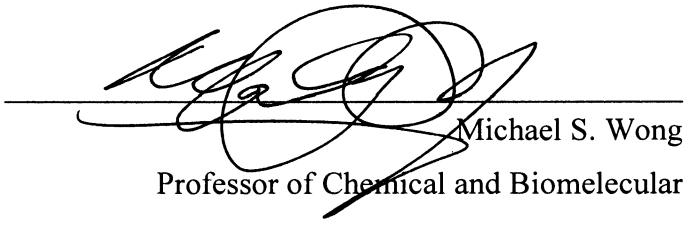

Michael S. Wong
Professor of Chemical and Biomelecular
Engineering and Chemistry

Houston, TX

September, 2011

# Abstract

**Regular Arrays of QDs by Solution Processing**

by

Brittany L. Oliva

Hydrophilic silicon and germanium quantum dots were synthesized by a "bottom-up" method utilizing micelles to control particle size. Liquid phase deposition of silica on these quantum dots was successful with and without DTAB (dodecyltrimethylammonium bromide) as a surfactant to yield uniform spheres. Coating the quantum dots in the presence of DTAB allowed for better size control. The silica coated quantum dots were then arrayed in three dimensions using a vertical deposition technique on quartz slides or ITO glass. UV-vis absorbance, AFM, SEM, and TEM images were used to analyze the particles at every stage. The photoconductivity of the arrays was tested, and the cells were found to be conductive in areas.

This is for Granny and Paw Paw who lost their battles during the making of this degree.

# Acknowledgements

I would like to first of all thank my mom for always being there for me throughout my entire life with encouragement, love, and support. I would like to thank my fiancé for all of your love and support through the long distance of deployments and military life; it has been a challenge, but some of the hard part is almost over. Since my family is not with me, my friends have been my family and have stood by me in the time I have spent here, and I would like to thank you for all of the moral support and advice through all of the rough spots. I would also like to thank all of the members of the Barron group, past and present, for helping me with any difficulty that I came across whether it was chemistry related or not; you are the best lab mates anyone could ask for. Finally, I would like to thank my advisor, Dr. Barron; I am not certain where I would be without you today. I could not have dreamed of a more understanding and patient advisor if I had the chance.

# Table of Contents

# List of Figures

**Introduction**

# List of Tables

# Abbreviations

| | |
|---|---|
| AFM | atomic force microscopy |
| AM | air mass |
| arb. units | arbitrary units |
| CBD | chemical bath deposition |
| CIGS | copper indium gallium diselenide |
| DSSC | dye-sensitized solar cell |
| DTAB | dodecyltrimethylammonium bromide |
| EGS | electronic grade silicon |
| eV | electron volts |
| $Ge@SiO_2$ | silica coated germanium quantum dot |
| HRTEM | high-resolution transmission electron microscopy |
| ITO | indium tin oxide |
| kV | kilovolts |
| LPD | liquid phase deposition |
| M | molar |
| mA | milliamps |
| MGS | metallurgical grade silicon |
| μL | microliter |
| μm | micrometer |
| mL | milliliter |
| mm | millimeter |
| mV | millivolts |
| nm | nanometer |
| Ω | omega, ohms |
| PVD | physical vapor deposition |

| | |
|---|---|
| QD | quantum dot |
| SEM | scanning electron microscopy |
| $Si@SiO_2$ | silica coated silicon quantum dot |
| $SiO_2$ | silica, silicon dioxide |
| TEM | transmission electron microscopy |
| TEOS | tetraethoxysilane |
| TOAB | tetraoctylammonium bromide |
| UV-vis | ultraviolet-visible |
| V | volts |
| XPS | X-ray photoelectron spectroscopy |

# Introduction

Ever since Becquerel discovered the first photovoltaic effect in 1839, harvesting solar energy has been a goal in the scientific world.[1,2] The earth's atmosphere absorbs more energy in one hour from the sun than the amount of energy consumed in one year for the entire world.[3] For this reason, research in the last few decades has exploded to find the most efficient and cost effective solar cell so the world does not remain oil dependant.

Solar cells need to absorb a range of energy, which corresponds to the solar spectrum to be efficient. The solar spectrum has a range of 100 nm to 1 mm, but as Figure I.1 shows, most of the irradiance occurs between 250 and 2500 nm with the maximum in the visible region of light (400 to 700 nm) for air mass (AM) 0, which means that solar cells should strive to absorb as much in the visible region of the solar spectrum as possible.[3-5]

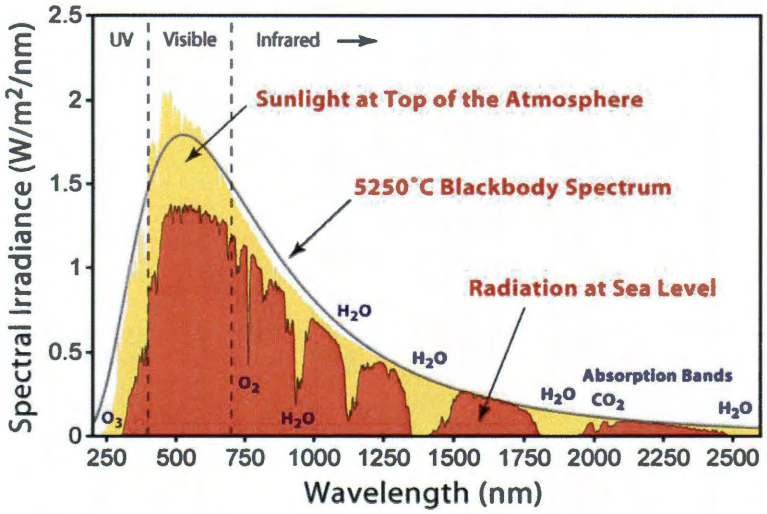


**Figure I.1.** Solar irradiance spectrum at AM 0 (Adapted from M. Pagliaro, G. Palmisano, and R. Ciriminna, *Flexible Solar Cells,* John Wiley, New York, 2008).

Air mass is the relative path length of light through the earth's atmosphere in relation to the zenith point (Figure I.2); the zenith point is the path length vertically upward at 90° and is defined as AM 1. Air mass 0 is above the atmosphere at the zenith point. Solar cells are tested at AM 1.5, which corresponds to the sun at a 48.2° angle from the zenith point, with a temperature of 25 °C.[5,6]

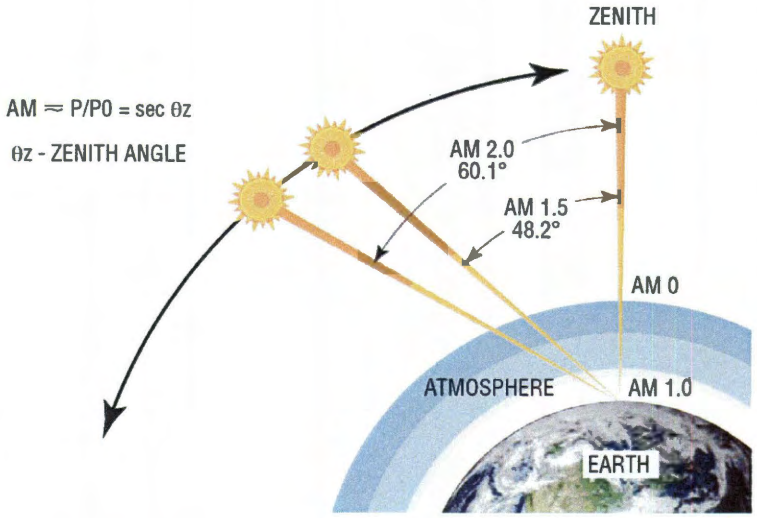


**Figure I.2.** Illustration of various air mass (AM) positions and the zenith point (Adapted from M. Pagliaro, G. Palmisano, and R. Ciriminna, *Flexible Solar Cells*, John Wiley, New York, 2008).

Solar cells are characterized in categories called generations, and these are usually defined as being in one of three generations. First generation solar cells are made of silicon wafers. This type of solar cell is the most widely used and manufactured in the world; they also have the highest reported single cell efficiencies. Silicon solar cells are expensive to produce, so research led the next generation of solar cells away from silicon. Second generation solar cells are called thin film solar cells.[2] These solar cells are made of thin film semiconductor materials such as copper indium gallium selenide ($CuIn_xGa_{1-x}Se_2$, CIGS) and cadmium telluride (CdTe); they are lower in cost compared to the silicon

cells, but they have environmental issues and the efficiencies are lower.[2,5,6] Third generation solar cells are much cheaper than all of the other cells, but their efficiencies are much lower than all other cells available. These solar cells are made of materials that do not have a strict p-n junction like first and second generation cells. Examples of third generation solar cells are dye-sensitized solar cells and organic or polymer solar cells. Table I.1 shows the highest reported efficiencies of each kind of solar cell along with a tandem cell. Tandem solar cells are cells, which have more than one p-n junction and more than one cell; they are generally used for space due to their high cost and efficiencies.

**Table I.1.** Solar cell efficiencies.[6]

| Solar Cell | Highest reported efficiency (%) |
|---|---|
| Silicon (single crystal, single cell) | 27.6 ±1.0 |
| CIGS (thin film, single cell) | 20.3 ±0.6 |
| CdTe (thin film, single cell) | 16.7 ±0.5 |
| Dye-sensitized (single cell) | 11.2 ±0.3 |
| Organic polymer (single cell) | 8.3 ±0.3 |
| InGaP/GaAs/InGaAs (tandem cell) | 42.3 ±2.5 |

**First generation silicon solar cells.** Bell Laboratories developed the first silicon solar cell in 1954 with an efficiency of 6%.[7] Since then, research on improving the efficiency and cost of these solar cells has been abundant. Silicon solar cells are the most widely used of all solar cells, and they are also the most efficient in terms of single cell photovoltaic devices, and it is the most abundant element on earth, only second to oxygen.[8] Silicon has an indirect band gap (Figure I.3) of 1.12 eV, which allows the material to absorb photons in the visible region of light.[9] An indirect band gap occurs

when the valence and conduction band edges are not aligned in $k$ space. $k$ space is a coordinate system, which is used for counting quantum states and describing band gaps.

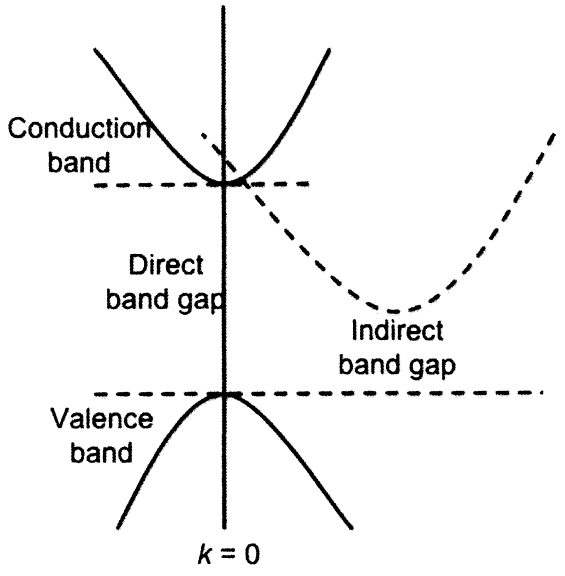


**Figure I.3.** Direct and indirect band gaps (Adapted from J. Singh, *Semiconductor Devices: Basic Principles*, John Wiley, New York, 2001).

There are three types of silicon used in first generation solar cells: single crystalline silicon, multicrystalline silicon, and amorphous silicon. Single crystalline silicon has the highest efficiency at about 28%, but it is the most expensive. Multicrystalline silicon has a lower efficiency at about 21%, but it is slightly less costly to produce. Amorphous silicon has a much lower efficiency at 16%, but it is much less expensive to make. Multicrystalline silicon is the most widely used commercially due to the efficiency and lower cost.[2,6]

The cost of fabricating single crystalline silicon solar cells is due to the purification process of bulk silicon into single crystals. To purify silicon, quartzite gravel, high purity silica, is melted and reduced using a carbon bed at a temperature above 1800 °C; this process makes the silicon 98 - 99% pure and is called metallurgical grade silicon

(MGS). MGS is then ground and reacted with hydrochloric acid at 300 °C to make trichlorosilane (TCS). The TCS is heated to 1100 °C in a hydrogen atmosphere to make electronic grade silicon (EGS); this final process makes the silicon 99.9999999% pure.[10]

A process is known as the Czochralski process is used commercially for single crystal silicon production (Figure I.4). In the Czochralski process, a small single crystalline silicon seed is inserted into molten EGS at a temperature above 1700 °C. The seed is continually twisted and slowly drawn out of the melted silicon, which allows the silicon atoms to attach to the seed and arrange in a single crystal lattice; this forms a uniform single crystalline ingot of silicon. Silicon wafers are sliced from the ingot. These wafers are then made smooth from the slicing by polishing them chemically and mechanically.[10]

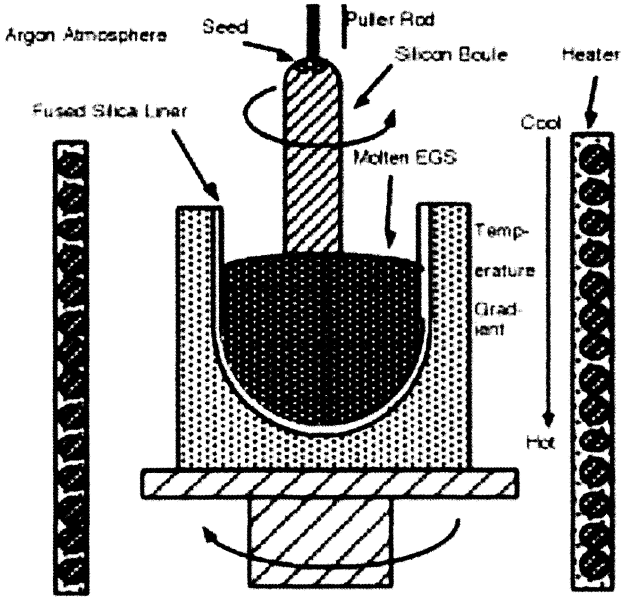


**Figure I.4.** Illustration of the Czochralski crystal growth process (Adapted from B. Wilson, *Silicon Growth*, Connexions web site, http://cnx.org/content/m1033/2.15/).

Multicrystalline silicon and amorphous silicon are much less pure than the single crystalline silicon, and their efficiencies reflect that. Amorphous silicon is prepared as a

thin film not as a crystal and will be discussed in the next section. Multicrystalline silicon is made by pouring molten silicon in a mold and allowing it to cool, and this process is called casting. The resulting silicon has no overall lattice structure, but the ingot produced has large column grains of crystallinity. The ingot is still sliced and treated as the single crystalline silicon ingot is treated except that the bottom and top of the ingot are removed before slicing due to poor crystallinity at the edges. The casting process is much cheaper and simpler than the Czochralski method used for single crystal growth.[11]

Silicon solar cells typically have two layers: a positive layer (p-type) and a negative layer (n-type). The positive layer is usually made by doping silicon with boron to create extra holes in the silicon lattice, and the negative layer is usually made by doping silicon with phosphorus to have extra electrons available in the silicon lattice. The two types of silicon are put into contact with each other and a p-n junction is formed at the boundary between them.[1] Figure I.5 illustrates what happens when electrons and holes are generated near the p-n junction of the solar cell; the electrons and holes diffuse into the n-type and p-type silicon respectively and form a neutral depletion region. Once the solar cell is exposed to light, or photons, of greater energy than the band gap of silicon (1.12 eV), an electron-hole pair is generated, and the cell starts converting solar energy into electricity.[2,12]

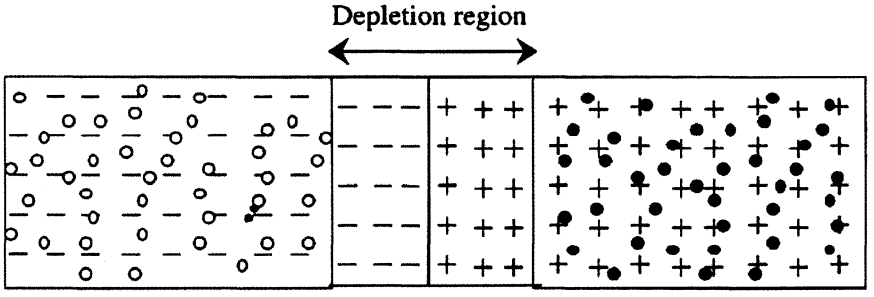


**Figure I.5.** Schematic of a p-n junction and the depletion region of a silicon solar cell (Adapted from T. Soga, *Nanostructured Materials for Solar Energy Conversion*, Elsevier, New York, 2006).

Several issues affect the efficiency of solar cells (Figure I.6):[5,13,14]

(1) The energy of the photons hitting the solar cell is less than the band gap, so the light cannot be converted into electricity and is lost.

(2) The energy of the incoming photons is greater than the band gap, so the excess energy is lost as heat.

(3) The Fermi levels of both n-type and p-type silicon are always inside the band gap of silicon so the open-circuit voltage is smaller than the band gap.

(4) The series and shunt resistors generated from the contacts and lattice defects in the silicon consume some of the electricity that is generated.

(5) Electron-hole pair recombination instead of conversion to electricity.

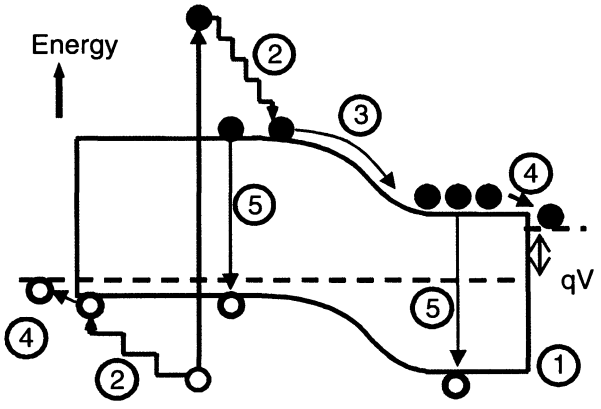


**Figure I.6.** Illustration of energy loss in a p-n junction silicon solar cell: (1) Unabsorbed light, (2) excess energy loss as heat, (3) Fermi level mismatch with band gap, (4) transfer loss, and (5) electron-hole recombination (Adapted from M. Pagliaro, G. Palmisano, and R. Ciriminna, *Flexible Solar Cells*, John Wiley, New York, 2008).

The cell also has an aluminum backing for energy transfer, an anti-reflective coating on top of the silicon to maximize use of the photons hitting the cell typically made of $SiN_x$ or $TiO_2$, silver conductor strips for energy transfer, followed by glass on

the top of the cell for protection from the elements. Figure I.7 illustrates the basic structure of a silicon solar cell.

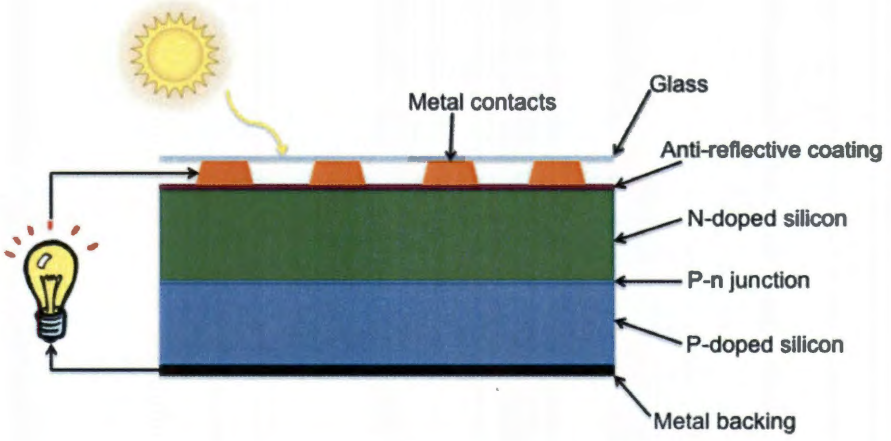


**Figure I.7.** Schematic of the basic structure of a silicon solar cell (Adapted from P. J. Reddy, *Science and Technology of Photovoltaics, 2nd edition,* CRC Press, Leiden, 2010).

Today, the highest efficiency reported for terrestrial solar cells is around 28%, which is relatively low; however, Shockley and Quissier reported the maximum efficiency of a single silicon cell is only 31%.[4,6,15] The efficiency of these solar cells is slowly reaching the theoretical maximum, which leaves little room for improvement, and because of this, different approaches to solar cells are investigated.

**Second generation thin film solar cells.** Thin film solar cells emerged due to their lower production costs and minimal material consumption, which makes these cells attractive to industry. There are three types of thin film cells: amorphous silicon, copper indium gallium diselenide ($CuIn_xGa_{1-x}Se_2$, CIGS), and cadmium telluride (CdTe).[2,5] Amorphous silicon is the most commercially used of these due to the fact that they can use existing silicon solar cell technology for manufacturing, but these cells have a couple of disadvantages. One disadvantage is that they do not absorb as efficiently as other

silicon solar cells, and the other is that these cells photodegrade over time. Because of these disadvantages, CIGS and CdTe thin film cells were developed due to their stability and efficiencies. These cells are also much less expensive to produce than amorphous silicon thin film cells.

There are a few fundamental differences between second generation solar cells and first generation solar cells. The most notable difference is the semiconductor material used in the cell has a direct band gap as opposed to the indirect band gap of silicon (Figure I.3), but these cells still rely on a p-n junction design. Thin film cells have a top layer called the winder layer made of a large band gap material that absorbs the higher energy photons and a bottom layer called the absorber layer made of a smaller band gap material that absorbs the lower energy photons, which are not absorbed by the window layer.[2,5] This design allows for an inherently better efficiency. CIGS cells have the highest efficiencies of thin film cells at 20%; CdTe cells have an efficiency of 17%, and amorphous silicon has an efficiency of 16%.[6]

CIGS has a direct band gap which is tunable depending on the ratio of Cu to (In + Ga) and the ratio of In to Ga; $CuInSe_2$ has a band gap of 1.0 eV while $CuGaSe_2$ has a band gap of 1.7 eV. The CIGS layer is the absorber layer of the thin film cell. Cadmium sulfide (CdS), with a larger direct band gap of 2.4 eV, is the window layer of this cell. CdS has been determined as the best window layer material, but ZnS, ZnSe, $In_2S_3$, ZnO, and MgZnO could also be used as window layer material.[2,5]

The basic structure of a CIGS thin film solar cell is illustrated in Figure I.8. The glass substrate is typically soda lime glass due to the fact that the sodium diffuses into the CIGS layer and increases conductivity and reduces the formation of lattice defects. Molybdenum (Mo) is used as a back contact for energy flow. The CIGS layer is deposited on the Mo by physical vapor deposition (PVD). A thin CdS layer is then deposited into the CIGS layer by chemical bath deposition (CBD). Both PVD and CBD must be performed at temperatures above 350 °C to ensure crystallinity. A high

resistance and low resistance bilayer of ZnO is sputtered onto the cell as transparent conductive oxides. Finally, nickel/aluminum (Ni/Al) contacts are added for energy flow. An anti-reflective coating of $MgF_2$ is added to maximize the absorption of the photons hitting the cell.[2,5]

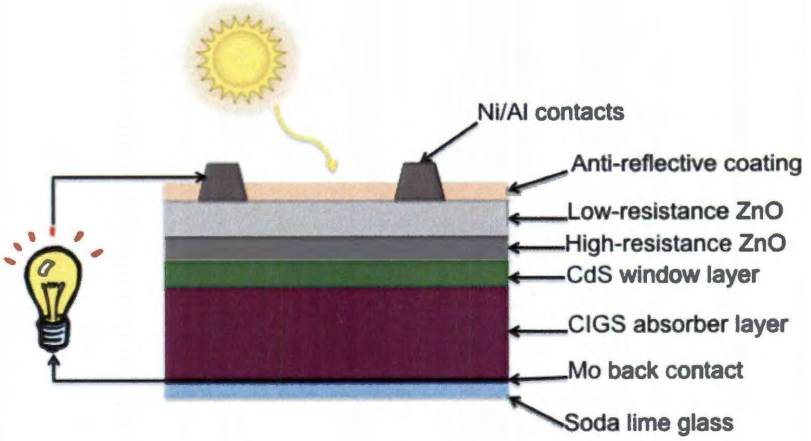


**Figure I.8.** Schematic of the basic structure of a CIGS solar cell (Adapted from P. J. Reddy, *Science and Technology of Photovoltaics, 2nd edition*, CRC Press, Leiden, 2010).

CdTe thin film cells are very similar to CIGS solar cells. CdTe has a direct band gap of 1.45 eV, and it is used as the absorber layer material. These cells also use CdS as the window layer material. Figure I.9 illustrates the basic structure of a CdTe solar cell. The glass substrate for this solar cell is typically soda lime glass coated with a thin conductive layer of tin oxide (SnO) or indium tin oxide (ITO). A thin film of CdS is deposited on the glass using the CBD method. The CdTe layer can then be deposited using several different methods; closed-space sublimation (CSS), PVD, electrodeposition, or spray pyrolysis are all methods of CdTe deposition and all require temperatures greater than 400 °C to ensure crystallinity. Finally, a back contact of Mo or W (tungsten) is deposited for conductivity.[2,5]

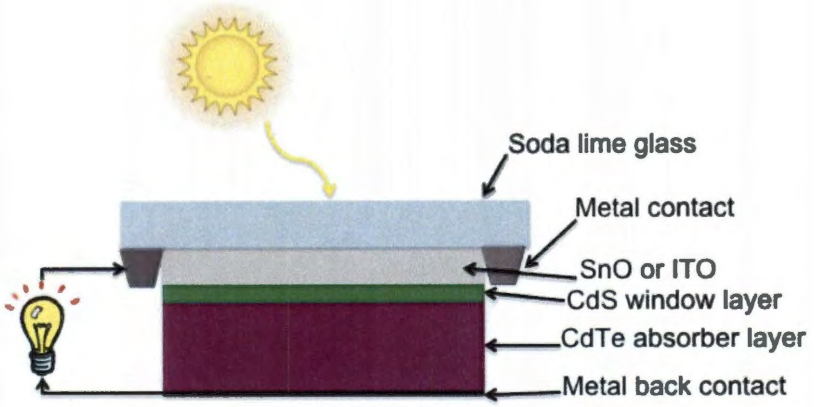


**Figure I.9.** Schematic of the basic structure of a CdTe solar cell (Adapted from P. J. Reddy, *Science and Technology of Photovoltaics, 2nd edition,* CRC Press, Leiden, 2010).

Although these thin film solar cells have a competitive edge on the first generation solar cells because of lower costs and good efficiencies, they have some drawbacks. Most of the material that these cells are made of are either becoming increasingly rare and more expensive (indium) or are highly toxic (cadmium). To mass produce these solar cells would also require new facilities, which would greatly increase the cost of production. Because of these drawbacks, a different generation of solar cells has been inspired.

**Third generation solar cells.** Due to high costs of first generation solar cells and toxicity and limited availability of materials for second generation solar cells, a new generation of solar cells emerged. Third generation solar cells are inherently different from the previous two generations because they do not rely on the p-n junction design of the others. There are a couple of popular models for third generation cells, which include dye-sensitized solar cells (DSSC) and organic or polymer solar cells.[2,5]

Dye-sensitized solar cells are also frequently called Grätzel cells named after the developer.[16-18] DSSCs separate the absorption of photons from the energy generation. An organometallic dye, which absorbs photons in the visible range, direct injects the

electrons generated from absorption into the band gap of a wide band gap semiconductor, and charge separation occurs at the interface of the dye and the semiconductor. The cell also contains an electrolyte to assist in hole transport.[16-18]

Figure I.10 illustrates the mechanism of a DSSC. The dye, typically based on ruthenium complexes, gets an electron from the iodide ions in the redox mediator iodide/triiodide ($I^-/I_3^-$) couple electrolyte. The reduction of the triiodide at the cathode, which completes the circuit, regenerates the iodide to make the process in this cell regenerative. The electron that the dye obtained from the electrolyte is then direct injected into the semiconductor, which is typically titanium dioxide ($TiO_2$) or zinc oxide (ZnO) with band gaps of 3.1 eV or 3.3 eV respectively. The injected electrons transfer to the conducting glass where the electrons are collected.[16-18]

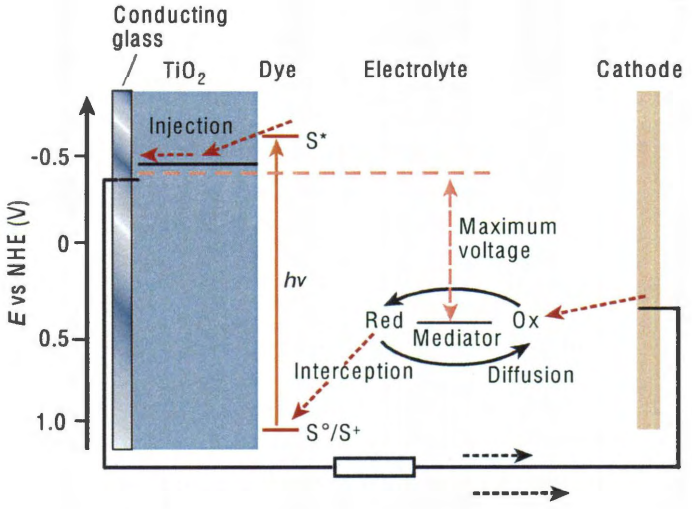


**Figure I.10.** Schematic of the mechanism of a DSSC (Adapted from M. Grätzel, *Nature*, 2001, **414**, 338).

Although the process in the DSSCs is reversible and regenerative, the highest efficiency reported for this type of cell is only 11%.[6] These cells are very inexpensive to

produce, but they photodegrade in a short period of time and the dyes tend to leak very easily, so other cell designs have been investigated for more ideal properties.

Organic or polymer solar cells were developed to make a more flexible solar cell. DSSCs are not considered organic because they use organometallic dyes and inorganic semiconductors. Organic or polymer cells are classified as such because the active layers of the cell are made of completely organic materials. These cells can either have a bilayer structure or a bulk-heterojunction structure, but the mechanism of both designs is the same.[17-19] The active layer of organic solar cells is comprised of donor and acceptor materials for charge separation and transportation. Figure I.11 illustrates the mechanism of an organic solar cell. The active layer could be made of a few different materials: small organic molecules, conjugated polymers, or combinations of molecules and polymers.[19] The cell is made of an aluminum electrode and conductive ITO glass with the active layer between the two materials with buffers to improve charge transportation. Photons are generally absorbed in the donor material to produce singlet excitons. These

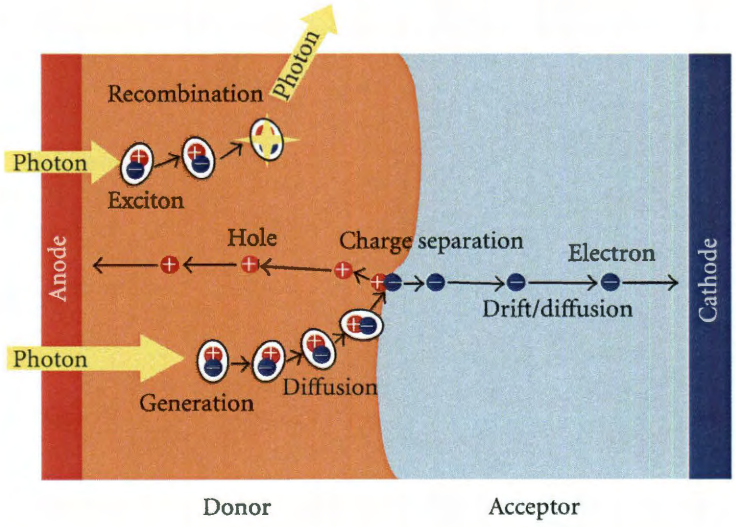


**Figure I.11.** Schematic of the mechanism of an organic solar cell (Adapted from T. Kietzke, *Adv. OptoElectron.*, 2007, **40285**, 1).

excitons migrate towards the acceptor material and separate into electrons and holes at the interface. The electrons and holes diffuse across the acceptor and donor materials respectively until they reach the electrodes. Typical materials for these cells are: phthalocyanines, fullerene ($C_{60}$), oliothiophenes, or polymers.[2,19]

In bilayer cells, electron-hole recombination is much less prevalent due to the fact that the electron and hole are separated at the interface of the material. This design has a flaw, however, because the bilayer only has one active zone, which is the interface. Because the excitons have to diffuse to the interface few of them go the distance, energy conversion is low. Bulk-heterojunction cells take care of this issue by having the donor and acceptor materials mixed throughout the active layer. Figure I.12 illustrates the design difference in the two cells. Because the acceptor and donor materials are so well mixed, the active zone for this cell is much larger; therefore, the energy conversion is much higher.[19]

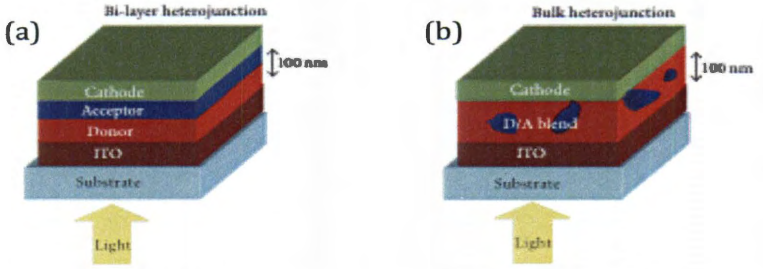


**Figure I.12.** Schematic of the basic structures of (a) bilayer and (b) bulk-heterojunction organic solar cells (Adapted from T. Kietzke, *Adv. OptoElectron.*, 2007, **40285**, 1).

Regardless of the design of the organic solar cell, the efficiency is not competitive with any of the other solar cell design options. The highest reported efficiency for these cells is 8%.[6] They are very inexpensive to build, which is an advantage, but the efficiencies are far too low to make these cells competitive in a commercial market.

**Multi-junction or tandem cells.** A tandem cell, by definition, consists of at least two p-n junctions with cells composed of materials that absorb different photon energies. The top cell would absorb the higher energies while the bottom cell would absorb the lower energies that were not absorbed by the top cell (Figure I.13), similar to the principle behind thin film cells. The tandem cell would then have a higher efficiency as it could absorb more photons of the solar spectrum for energy conversion. This technology is already being put to use in solar cells in space.[2,5] Tandem solar cells are typically made of compounds of elements in the III and V groups of the periodic tables. Examples of these compounds are: gallium arsenide (GaAs), indium phosphide (InP), gallium antimonide (GaSb), gallium indium phosphide (GaInP), and gallium indium arsenide (GaInAs). These solar cells have the highest reported efficiency at 43% when using a three cell solar cell, but they use rare metals and are extremely expensive to fabricate, so they are not practical for use on widespread earth.[6]

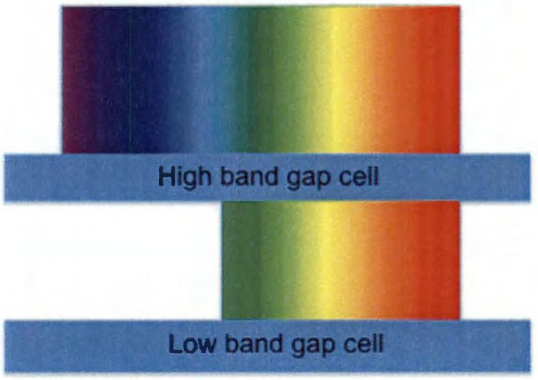


**Figure I.13.** Schematic of the absorbance of a two cell tandem solar cell where the top cell absorbs higher energy photons and the lower energy photons pass through to be absorbed by the bottom cell.

Increased number of cells in a tandem cell will increase the theoretical maximum efficiency of the solar cell, but there still remains a limit to the efficiency. A single cell

has a theoretical maximum efficiency of 31%.[15] A two cell tandem solar cell has a maximum efficiency of 42.5%; a three cell solar cell has a maximum efficiency of 48.6%, and so on. The theoretical maximum efficiencies will continue to increase, but an infinite stack of solar cells has a maximum efficiency of only 68.2%. The efficiency gained by adding another cell decreases with each subsequent addition.[5]

Green and coworkers in Australia have researched creating a tandem cell using a first generation multicrystalline silicon cell as the bottom cell.[13,14,20] The idea of a tandem cell using the original first generation solar cell would make for an easier transition in production. To improve on the existing silicon solar cells, the additions should not be expensive, toxic, or rare. Previous research has suggested that producing uniform silicon quantum dots in a matrix of silica as a top cell for the terrestrial silicon solar cell could improve efficiency by 20% (Figure I.14).[13,14,20]

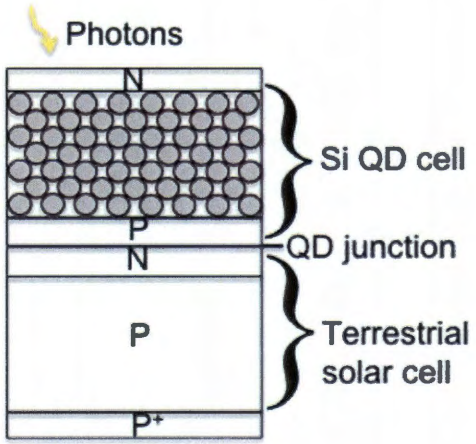


**Figure I.14.** Schematic of a tandem solar cell using a first generation silicon solar cell and a cell comprised of silicon quantum dots in a silica matrix (Adapted from E.-C. Cho, M. A. Green, G. Conibeer, D. Song, Y.-H. Cho, G. Scardera, S. Huang, S. Park, X. J. Hao, Y. Huang, and L. V. Dao, *Adv. OptoElectron.*, 2007, **69578**, 1).

Green *et al.* attempted to make the quantum dot cell by using an existing silicon wafer and chemically altering it to produce silicon quantum dots and a silica dielectric matrix.[14] The results of this method are not consistent in terms of quantum dot size or spacing, and they could not determine a way to control either of these parameters effectively using the methods they employed.[13,14,20] The goal of this project is to synthesize uniform silicon quantum dots, coat them in a uniform thickness of silica, and array them in such away that the quantum dots are evenly spaced. This would make up the tandem cell for an existing silicon solar cell.

## References


1. E. Becquerel, *C. R.*, 1839, **9**, 561.
2. P. J. Reddy, *Science and Technology of Photovoltaics, 2nd edition,* CRC Press, Leiden, 2010.
3. R. Foster, M. Ghassemi, and A. Cota, *Solar Energy: Renewable Energy and the Environment,* CRC Press, Boca Raton, 2009.
4. A. J. Nozik, *Physica E,* 2002, **14**, 115.
5. M. Pagliaro, G. Palmisano, and R. Ciriminna, *Flexible Solar Cells,* John Wiley, New York, 2008.
6. M. A. Green, K. Emery, Y. Hishikawa, and W. Warta, *Prog. Photovolt. Res. Appl.,* 2011, **19**, 84.
7. J. H. Felker, US Patent 2,670.445. 1954.
8. A. R. Barron, C. E. Hamilton, and C. Smith, *Chemistry of the Main Group Elements*, Connexions web site, http://cnx.org/content/col11124/1.25/.
9. J. Singh, *Semiconductor Devices: Basic Principles,* John Wiley, New York, 2001.
10. B. Wilson, *Silicon Growth*, Connexions web site, http://cnx.org/content/m1033/2.15/.

11. A. R. Barron, P.-T. Chiang, C. E. Hamilton, J. Holden, C. Kelty, I. Kurganskaya, A. Luttge, A. Saha, C. Smith, E. Whitsitt, and B. Wilson, *Chemistry of Electronic Materials*, Connexions web site, http://cnx.org/content/col10719/1.6/.

12. T. Soga, *Nanostructured Materials for Solar Energy Conversion,* Elsevier, New York, 2006.

13. E.-C. Cho, M. A. Green, G. Conibeer, D. Song, Y.-H. Cho, G. Scardera, S. Huang, S. Park, X. J. Hao, Y. Huang, and L. V. Dao, *Adv. OptoElectron.,* 2007, **69578**, 1.

14. G. Conibeer, M. Green, R. Corkish, Y. Cho, E.-C. Cho, C.-W. Jiang, T. Fangsuwannarak, E. Pink, Y. Huang, T. Puzzer, T. Truple, B. Richards, A. Shalav, and K.-L. Lin, *Thin Solid Films,* 2006, **511-512**, 654.

15. W. Shockley and H. J. Queisser, *J. Appl. Phys.,* 1961, **32**, 510.

16. M. Grätzel, *J. Photochem. Photobiol. C,* 2003, **4**, 145.

17. M. Grätzel, *Nature*, 2001, **414**, 338.

18. A. Hagfeldt and M. Grätzel, *Chem. Rev.,* 1995, **95**, 49.

19. T. Kietzke, *Adv. OptoElectron.*, 2007, **40285**, 1.

20. E.-C. Cho, M. A. Green, J. Xia, and R. Corkish, *Appl. Phys. Lett.*, 2004, **84**, 2286.

# Chapter 1
# Dielectric Coated Quantum Dots

## Introduction

Quantum confinement is a change of electronic properties of a given material below a certain size. This occurs when the overall size of the particle is smaller than the localization range of an electron in that material (also known as the Bohr radius).[1] Quantum confinement in very small semiconductor particles (known as quantum dots) has led to interesting optical properties that can be used in a wide range of photonic applications; however, much of the interest lies in improving solar cell efficiencies.[2,3] The Bohr radius of silicon is 4 nm, which means that a quantum dot of pure silicon must be less than 4 nm to exploit the quantum confinement effects of silicon (Figure 1.1).[2-4]

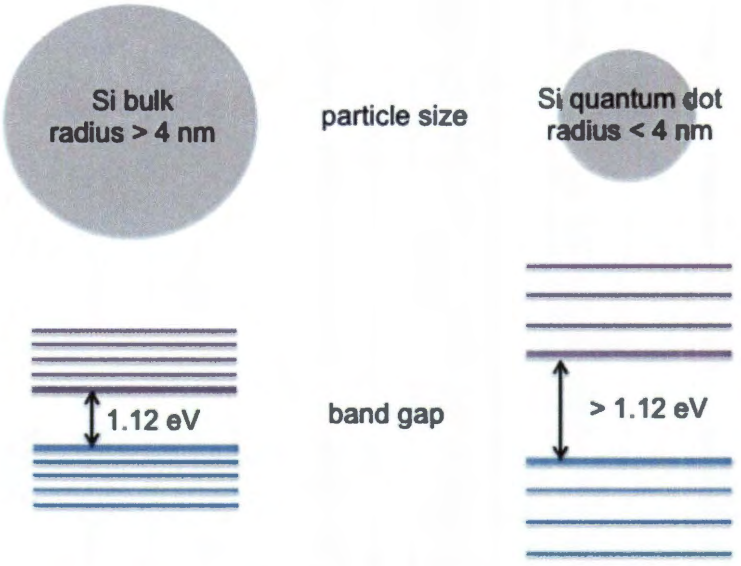


**Figure 1.1.** Schematic of the quantum confinement of silicon (Adapted from H. S. Mansur, *WIREs Nanomed. Nanobiotechnol.*, 2010, **2**, 113).

Silicon is of particular interest as a quantum dot compared to CdSe or PbS quantum dots because silicon is non-toxic, inexpensive, and widely available being the

second most abundant element (only after oxygen) in the earth's crust at 28%. Silicon is also the material that most commercial solar cell manufacturers use, so adding the silicon quantum dots to manufacturing should not require significant alteration in the present fabrication facilities.[5,6]

Bulk silicon has an indirect band gap of 1.12 eV, but once the radius of the silicon is below the Bohr radius, the band gap increases (Figure 1.1).[7] An indirect band gap occurs when the conduction and valence band edges are not aligned in *k* space (Figure I.3).[7] The band gap has been observed as being the same as bulk silicon until the radius is below 2 nm. For particles smaller than this, the band gap increases with decreasing size, but there is no firm data of a specific band gap associated with a specific size quantum dot.[4,6,8] Germanium has very similar properties to silicon with an indirect band gap of 0.66 eV and Bohr radius of 11.5 nm.[67,9,10] The larger Bohr radius makes germanium quantum dots ideal for further analysis and characterization because the synthesis of particles with quantum confinement is easier.

Silicon quantum dots embedded in silica has been of interest in recent years due to the fact that this material would make an efficient tandem cell for the first generation silicon solar cell. With a band gap of 8.9 eV, silica makes an ideal insulating matrix for the quantum dots to be arranged in, and because of the low interface densities of silicon and silica, there is very little electron or hole trapping.[7,11]

The research for quantum dots embedded in silica thus far has not been successful in synthesizing monodispersed quantum dots or in arraying them uniformly. The largest obstacle in this project is having the quantum dots close enough together in the silica matrix so that the electrons can transfer easily. For the tandem cell to be efficient, the quantum dots are required to be no more than 10 nm apart for good electron flow and low electron-hole recombination.[4] There are two methods of making quantum dots: bottom up (building up atom by atom) or top down (breaking down from bulk materials).[4] Most research has gone towards making silicon quantum dots top down in silica wafers so the

quantum dots would already be embedded in silica. Previous research synthesized quantum dots in a silicon wafer via chemical etching or laser ablation, but the result of working backwards, in a top down method, is that the quantum dots are not monodispersed, and they are not uniformly distributed in the matrix.[11,12] There is no way to control either of those problems using top down methods of synthesis; therefore, a bottom up approach is proposed here synthesizing quantum dots first then coating them with silica via liquid phase deposition (LPD) (Figure 1.2).

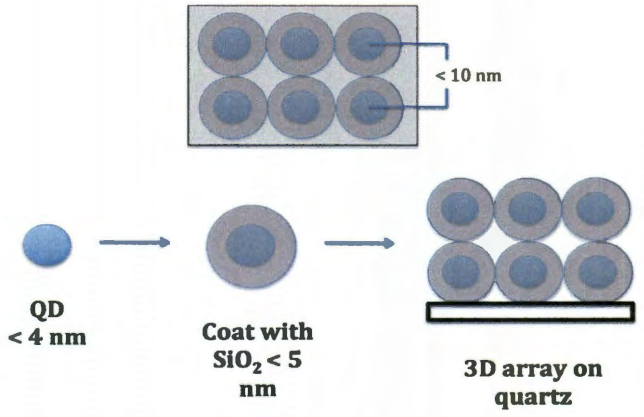


**Figure 1.2.** Schematic of overall project goal.

LPD is used as the method for silica coating because it does not require a vacuum, glove box, or high temperature, and because of this, it would not add much cost to fabrication of solar cells.[14] LPD was also chosen for the silica coating because it can be performed on non-planar surfaces, which is necessary for the quantum dots. LPD is the growth of silica from a fluorosilicic acid solution. The overall LPD reaction for silica is shown in Eq 1.1. The water in the reaction is what controls the growth rate of the silica.[14]

$$H_2SiF_6 + 2\ H_2O \rightleftharpoons SiO_2 + 6\ HF \qquad (1.1)$$

Silica growth on particles which have a hydroxyl (-OH) group has been proven. Because these particles have an elecrtonegative capping ligand, quantum dots with an electronegative coating should seed the growth of silica on the surface. The goal of this project is to synthesize monodispersed silicon quantum dots and uniformly coat them in a thin layer of silica using a liquid phase deposition (LPD) method and put them in an array (Figure 1.2).[14-16]

## Results and Discussion

**Silicon quantum dots.** Using a modification of a literature synthesis, size controlled, uniform silicon quantum dots were synthesized utilizing a reverse micelle reaction with tetraoctylammonium bromide (TOAB, Figure 1.3) as the surfactant in toluene, silicon tetrachloride ($SiCl_4$) as the silicon source, and lithium aluminum hydride ($LiAlH_4$) as a reducing agent.[3] Equation 1.2 is the basic reaction of forming silicon in this synthesis.

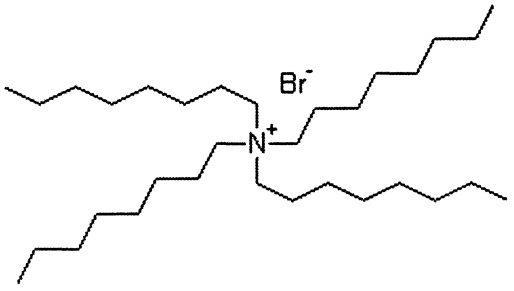


**Figure 1.3.** Structure of tetraoctylammonium bromide (TOAB).

$$SiCl_4 + LiAlH_4 \rightarrow Si + LiCl + AlCl_3 \qquad (1.2)$$

The particles are initially capped with hydrogen making them hydrophobic. These nanoparticles were then made hydrophilic by using a platinum catalyst and allylamine for further experimentation (Figure 1.4).

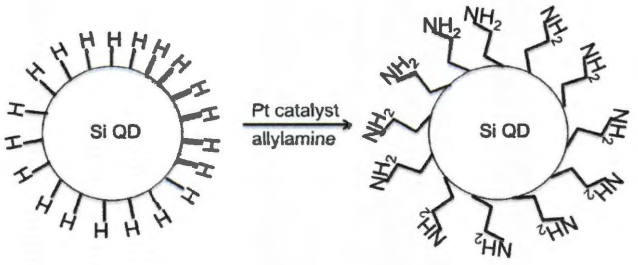


**Figure 1.4**. Reaction making hydrophobic quantum dots hydrophilic (Adapted from J. H. Warner, A. Hoshino, K. Yammamoto, and R. D. Tilley, *Angew. Chem., Int. Ed.*, 2005, **44**, 4550).

After the quantum dots were suspended in water and filtered, the solution appears as though it is water only with no obvious color or change in viscosity. To determine if quantum dots were in fact in the filtered water, UV-visible absorbance of the solution was measured (Figure 1.5). Absorbance is a valuable characteristic of nanoparticles. The ability of semiconductor nanoparticles to be altered in size or shape to evoke a different response to light is a property that is not available for bulk materials.[17] The absorbance of

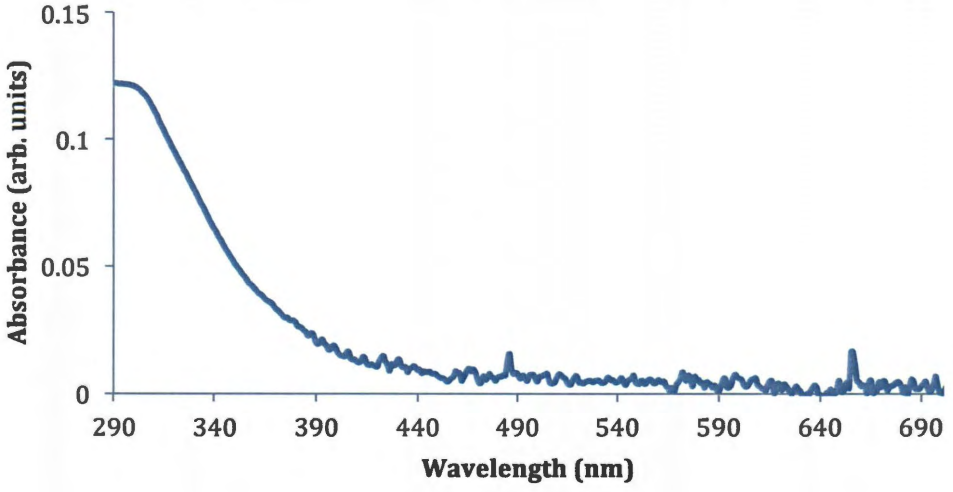


**Figure 1.5.** UV-visible spectrum of synthesized Si QDs.

the synthesized silicon quantum dots is 300 nm just as reported in literature.[3] Table 1.1 compares the absorbance and size of quantum dots analyzed here.

**Table 1.1**. Quantum dot data comparison.

| Element | Wavelength (nm) | Diameter (nm) from AFM |
|---|---|---|
| silicon/ synthesized | 300 | 0.9 ±0.2 |
| silicon/ commercial | 450 | 1.6 ±0.6 |
| germanium/ synthesized | 350 | 2.7 ±0.6 |
| germanium/ commercial | 260 | 0.9 ±0.4 |

Silicon quantum dots (5 nm) were also obtained from Universal Nanotech Corporation for comparison of the synthesized quantum dots to commercial quantum dots. These particles come concentrated in acetonitrile, so they were sonciated for several minutes and diluted 40-fold in deionized water for further experimentation and analysis. Absorbance of these particles was measured (Figure 1.6), and the spectrum of these particles indicates that they are greater than 2 nm in size.

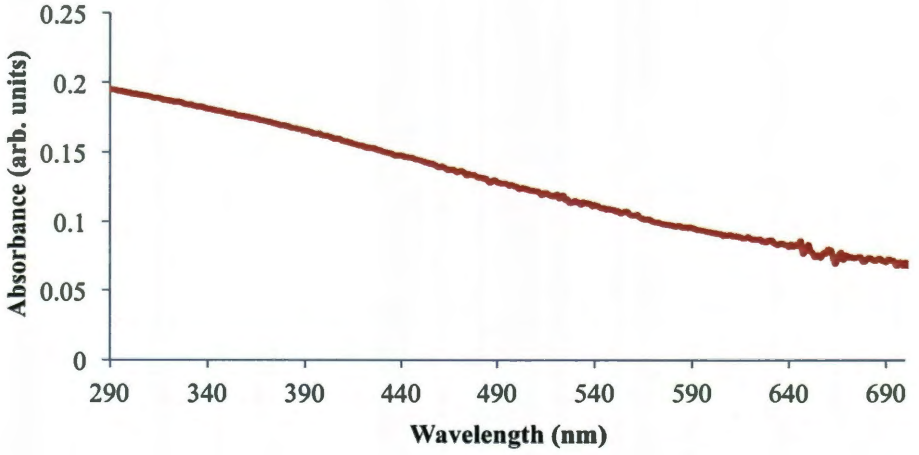


**Figure 1.6.** UV-visible spectrum of commercial Si QDs.

The sizes of the QDs can be determined by AFM, as can the shape of these particles. The AFM image of as synthesized quantum dots (Figure 1.7) indicates that the particles are uniform in size and shape. Based on several AFM images, the average size of the silicon quantum dots is 0.9 ±0.2 nm, and they are spherical in shape (Table 1.1). The average size of these particles is a little smaller than the reported average at 1.1 ±0.2

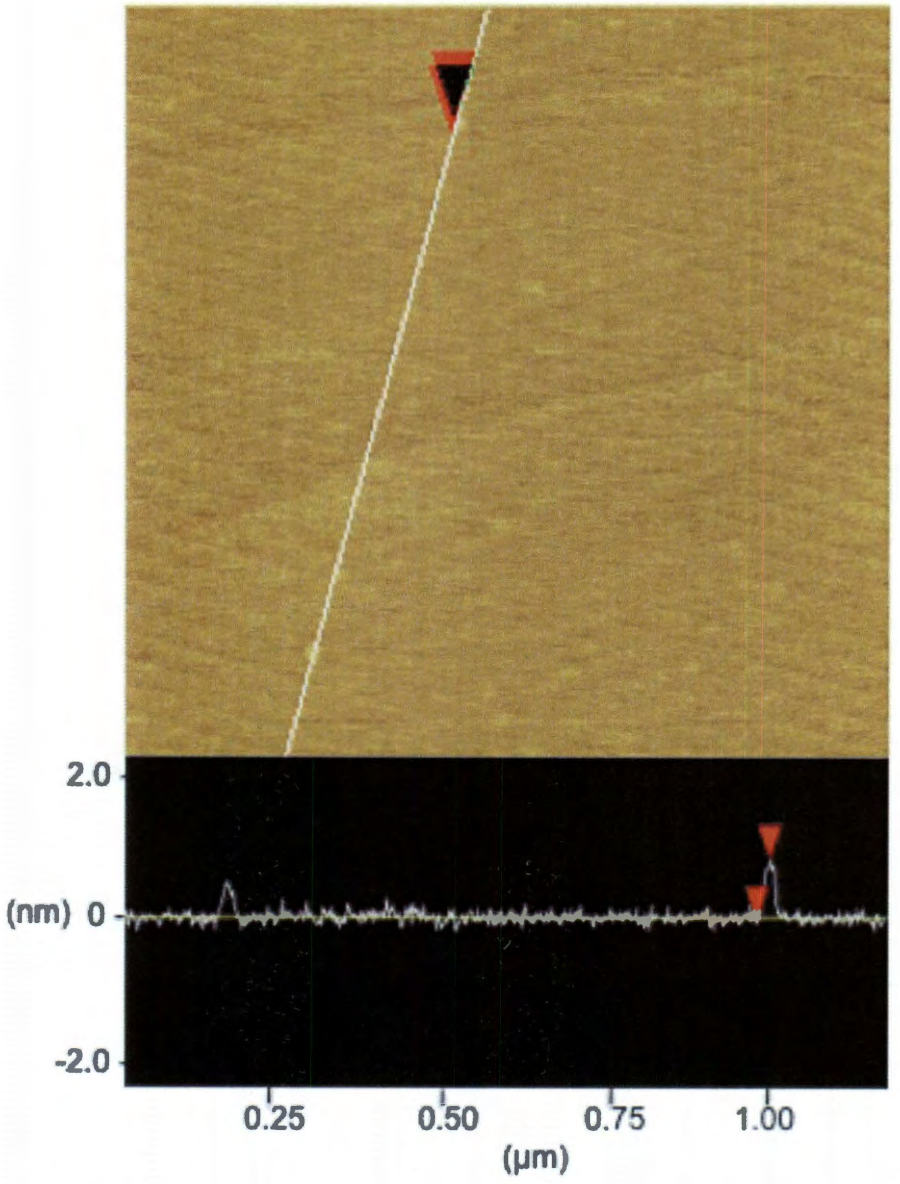


**Figure 1.7.** Tapping AFM image (1.2 x 1.2 μm) and associated height analysis of synthesized Si QDs.

nm, and there is no obvious explanation for this size discrepancy, but as long as the particles are less than 2 nm they are appropriate for our requirements.[3]

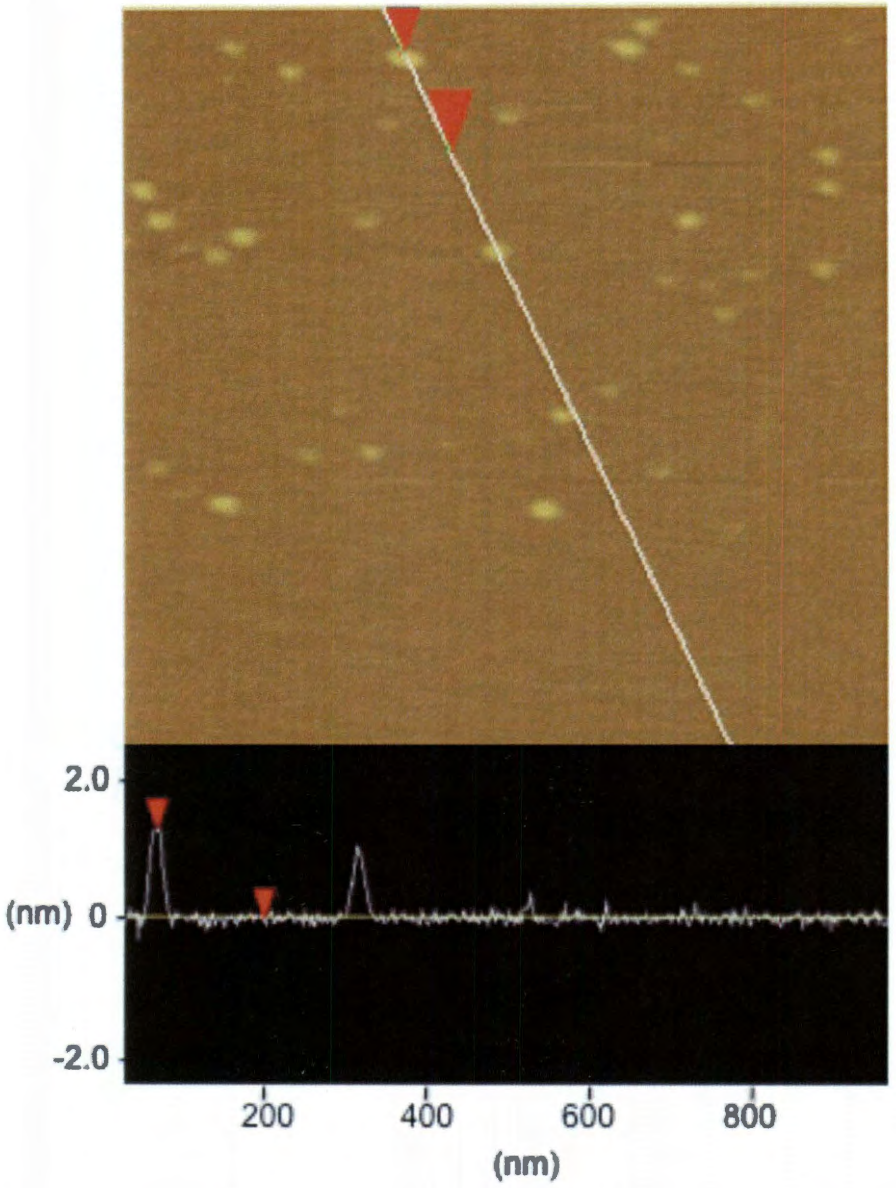


**Figure 1.8.** Tapping AFM image (1 x 1 μm) and associated height analysis of commercial Si QDs.

The commercial Si QDs are shown as being larger than the synthesized Si QDs. A typical AFM image is shown in Figure 1.8. The absorbance of these particles indicates

that they were larger than the synthesized QDs, and the manufacturer claims that they are 5 nm; however the AFM does not agree with the manufacturer. The commercial quantum dots are shown to have a larger size distribution than the synthesized QDs at 1.6 ±0.6 nm (Table 1.1).

**Germanium quantum dots.** Germanium quantum dots were synthesized in the same manner as the silicon quantum dots; germanium tetrachloride ($GeCl_4$) was used as the germanium source for these particles. The properties of germanium quantum dots are not well defined in other publications; however, the particles are typically reported to absorb at a higher wavelength and have an overall larger diameter than silicon quantum dots.[9] After the quantum dots were suspended in water and filtered, the solution appeared to be a very pale yellow color to the naked eye (Figure 1.9).

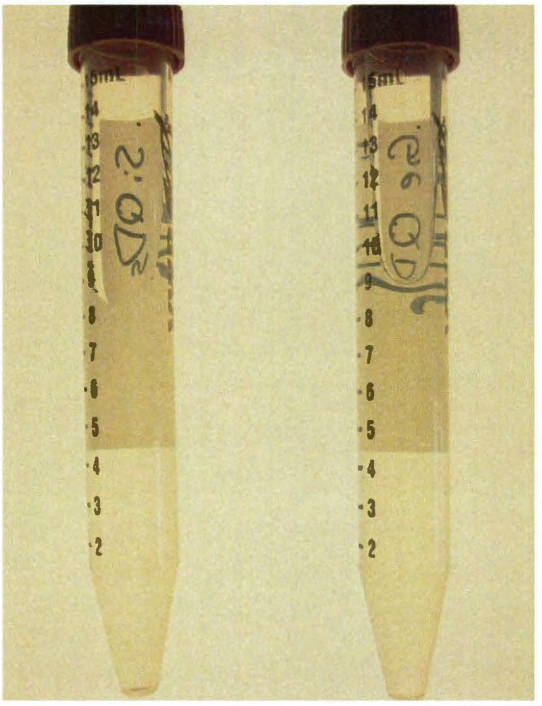

**Figure 1.9.** Photograph of silicon quantum dots in water (left) and germanium quantum dots in water (right).

After acquiring a UV-visible spectrum of the solution (Figure 1.10), it is clear that the particles do absorb in the visible region of the electromagnetic spectrum. The yellow tint is expected according to literature, but UV-visible absorbance data for these particles is not reported.

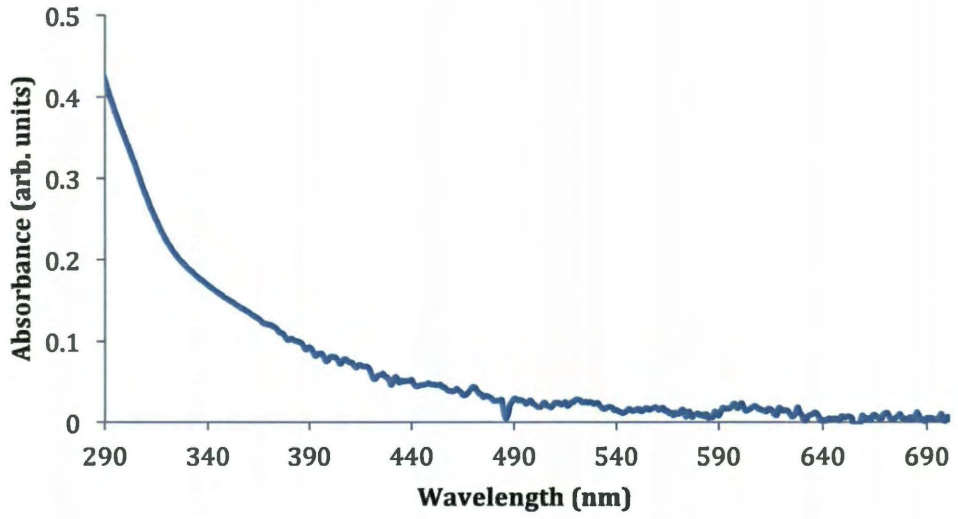


**Figure 1.10.** UV-visible spectrum of sythesized Ge QDs.

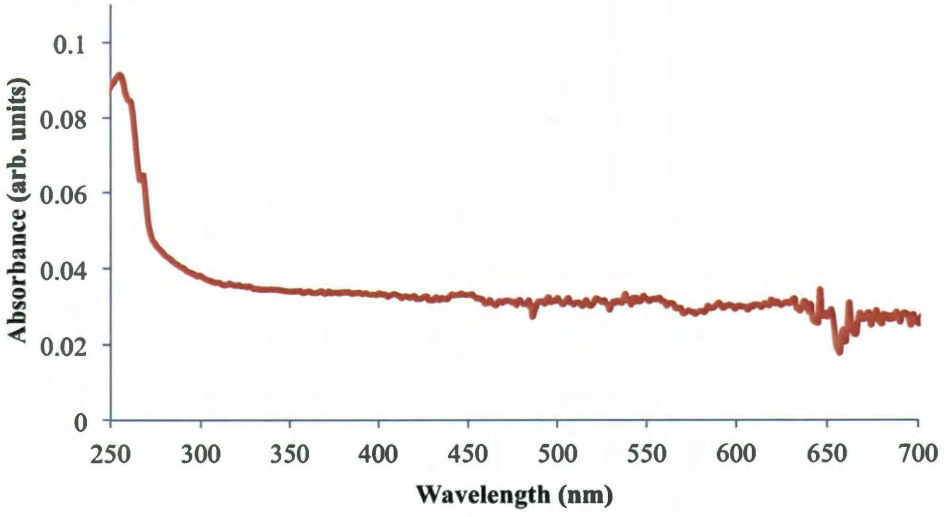


**Figure 1.11.** UV-visible spectrum of commercially available Ge QDs.

Germanium quantum dots (20 nm) were also obtained from Universal Nanotech Corporation for a comparison of lab made quantum dots to commercial quantum dots. These paricles also came concentrated in methanol, so they were sonicated for several

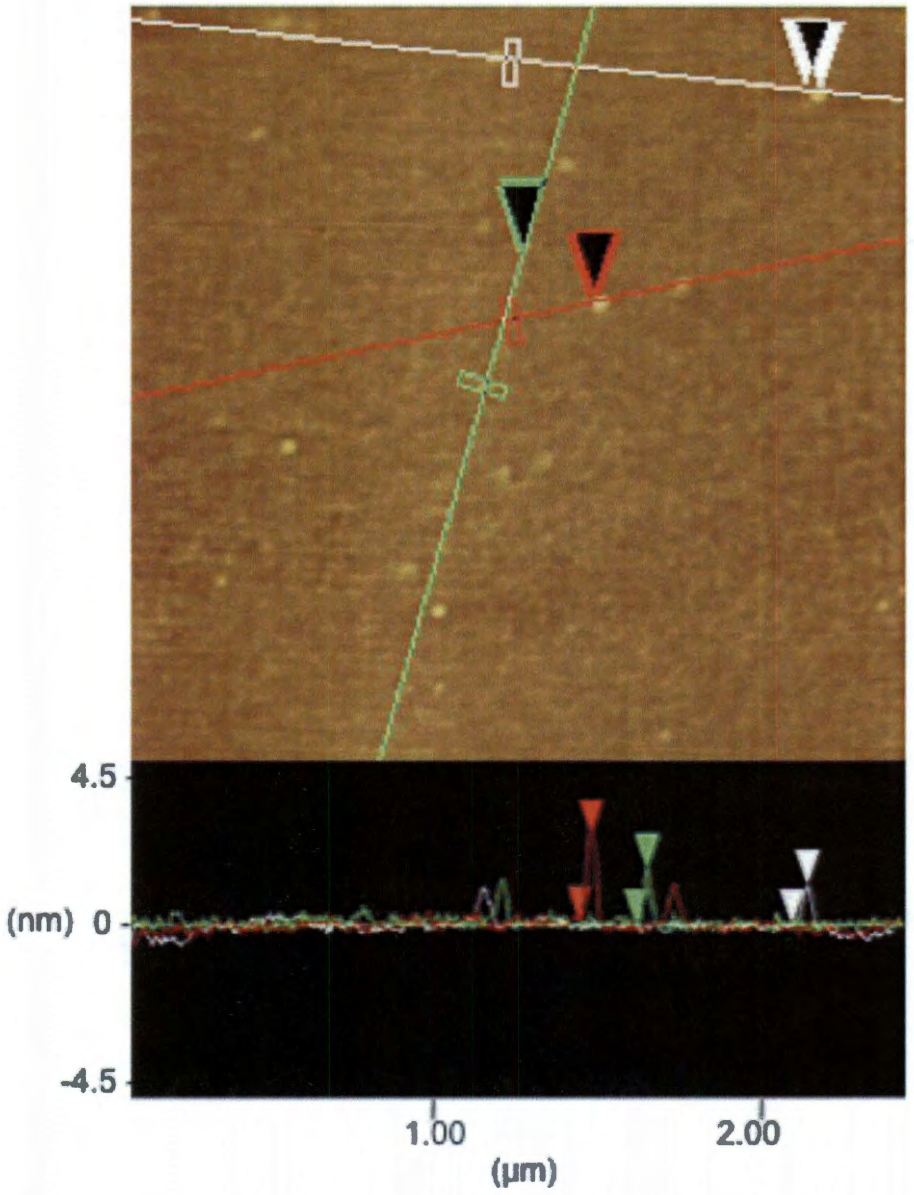


**Figure 1.12.** Tapping AFM image (2.4 x 2.4 µm) and associated height analysis of sythesized Ge QDs.

minutes and diluted 40-fold in dionized water for further analysis and experimentation. The absorbance spectrum of these particles (Figure 1.11) suggests that they are very small because the absorbance is in the ultraviolet region of the electronmagnetic spectrum.

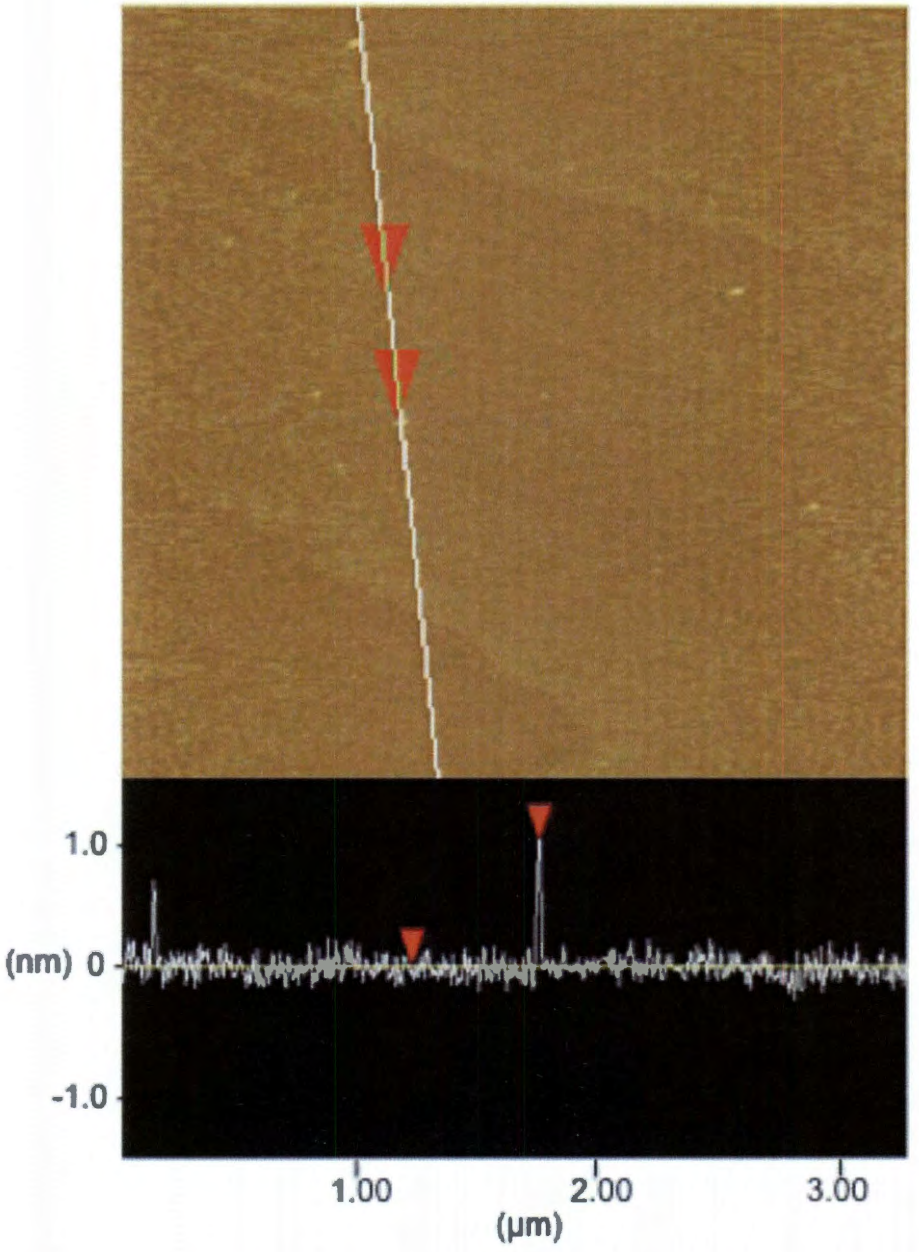


**Figure 1.13.** Tapping AFM image (4.1 x 4.1 μm) and associated height analysis of commercial Ge QDs.

After UV-vis was measured of the as synthesized quantum dots, AFM images were taken of the same material (Figure 1.12) to determine the size and shape of the particles in the sample. The AFM images indicate uniformity in shape and size of the silicon quantum dots as spherical particles, but the germanium nanoparticles were slightly less monodispersed than the silicon quantum dots. Synthesized Ge QDs are sized at 2.7 ±0.6 nm from tapping AFM images (Table 1.1).

The AFM of commercially available germanium quantum dots is shown in Figure 1.13. They are much smaller than synthesized Ge QDs at 0.8 ±0.2 nm (Table 1.1). The size of these particles coinsides with the absorbance spectrum very well.

**Silica coated silicon quantum dots.** Silica coating particles, instead of surfaces, using a liquid phase deposition (LPD) method has been previously reported for coating fullerenol, which was used as a seed particle for the silica to grow.[15] In these experiments, the quantum dots would be used as the seed particles for the silica deposition. Figures 1.14 (a) and (b) show TEM images of $Si@SiO_2$ particles synthesized with a 3 hr reaction time at 30 °C (Eq 1.3).

$$SiQDs + H_2SiF_6 + 2\ H_2O \rightleftharpoons Si@SiO_2 + 6\ HF \qquad (1.3)$$

These coated particles are perfectly spherical at 100 ±6 nm. This result is very impressive because the coating was successful using the quantum dots as the seed particles; however, the silica coating on the quantum dots needs to be 10 nm or less to not affect the efficiency of electron transfer.[4]

The silica deposition is reported at being linear with time; so another coating was made using only 15 minutes of reaction time (Figure 1.15) with all other parameters the same as those used in the previous reaction.[13] The coating was much thinner, and all of the particles looked very similar to the particle in Figure 1.15. This coating is not ideal

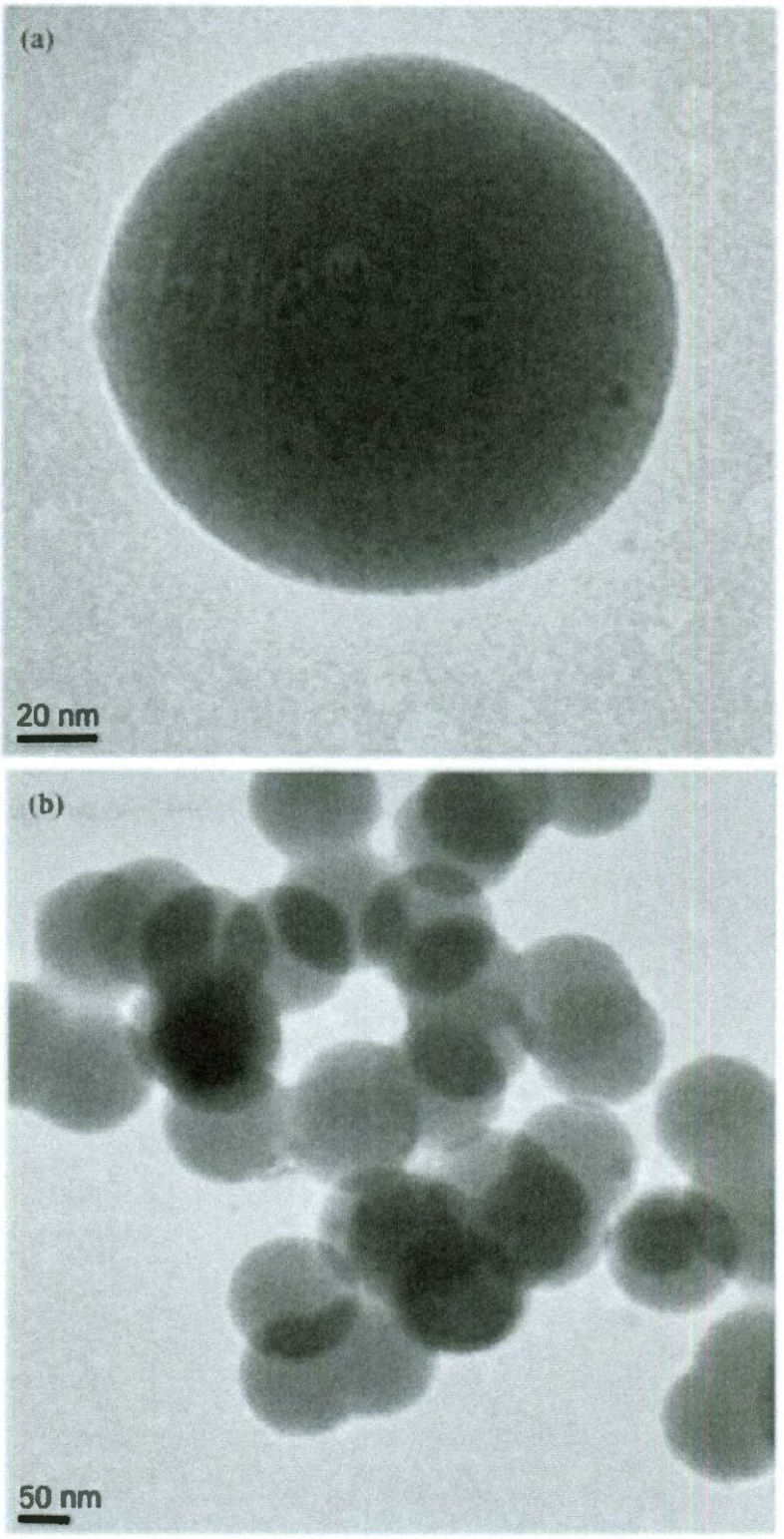


**Figure 1.14**. TEM images of $Si@SiO_2$ particles synthesized using a 3 hour reaction time.

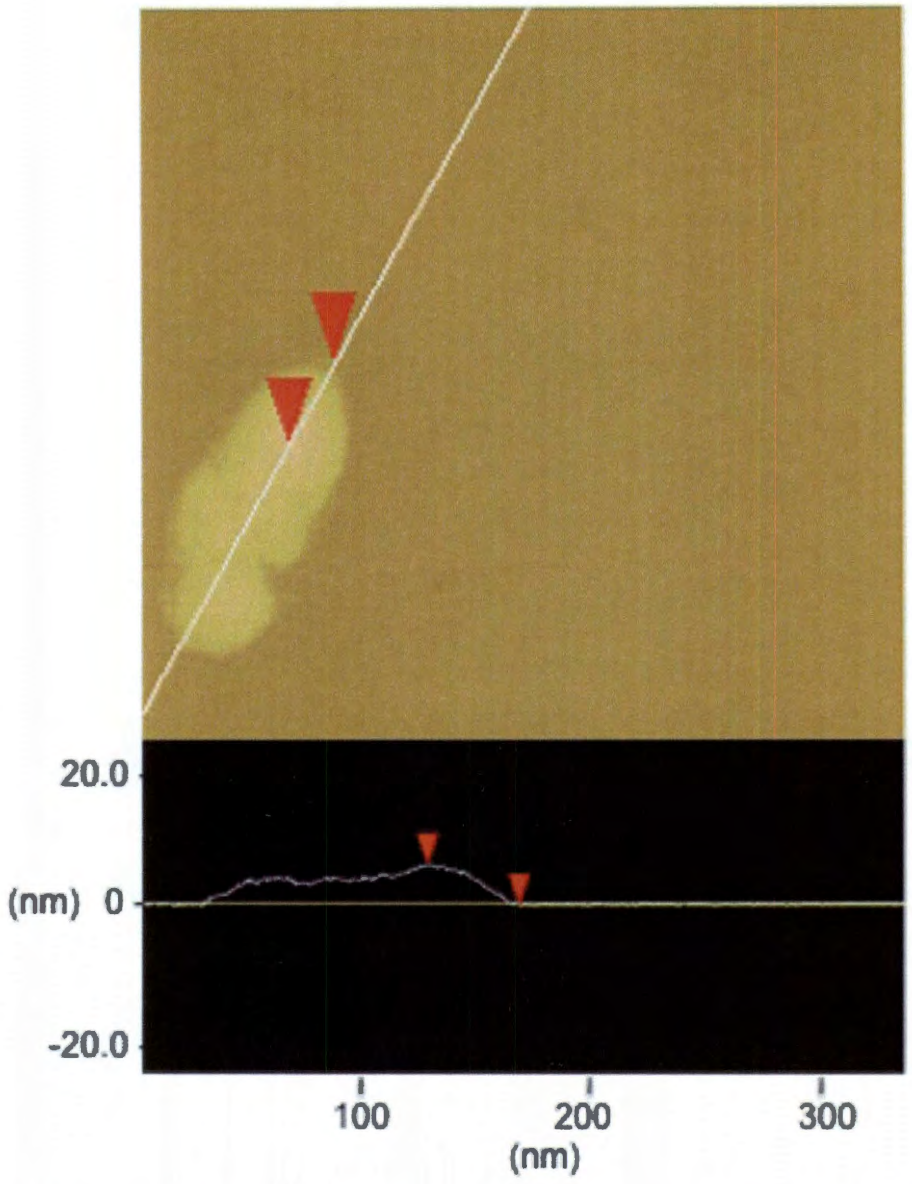


**Figure 1.15**. Tapping AFM image (320 x 320 nm) and associated height analysis of $Si@SiO_2$ particles synthesized using a 15 minute reaction time.

though; it is not uniform in shape or size. The diameter of these particles is 10 nm, which is a step in the right direction, but the shape is not conducive to good electron flow.

Synthesizing monodispersed silica spheres without a seed particle has also been reported with the aid of dodecyltrimethylammonium bromide (DTAB) (Figure 1.16) as a surfactant.[16] However, the silica coating with DTAB is reported to require a slightly

higher reaction temperature (40 °C), so instead of raising the temperature to get the silica to precipitate, the same temperature used in the seeded growth (30 °C) is used to ensure the quantum dots are in the silica and not just on their own in solution.

For the next set of experiments, DTAB was added to the solution to synthesize spherical particles. The first DTAB experiment reacted for 24 hours, and a TEM image of those particles is shown in Figure 1.17. The 24 hour DTAB coating is just as thick as the coating without DTAB at about 100 nm, which suggests that less reaction time is required to make a thinner coating of silica.


**Figure 1.16.** Structure of dodecyltrimethylammonium bromide (DTAB).

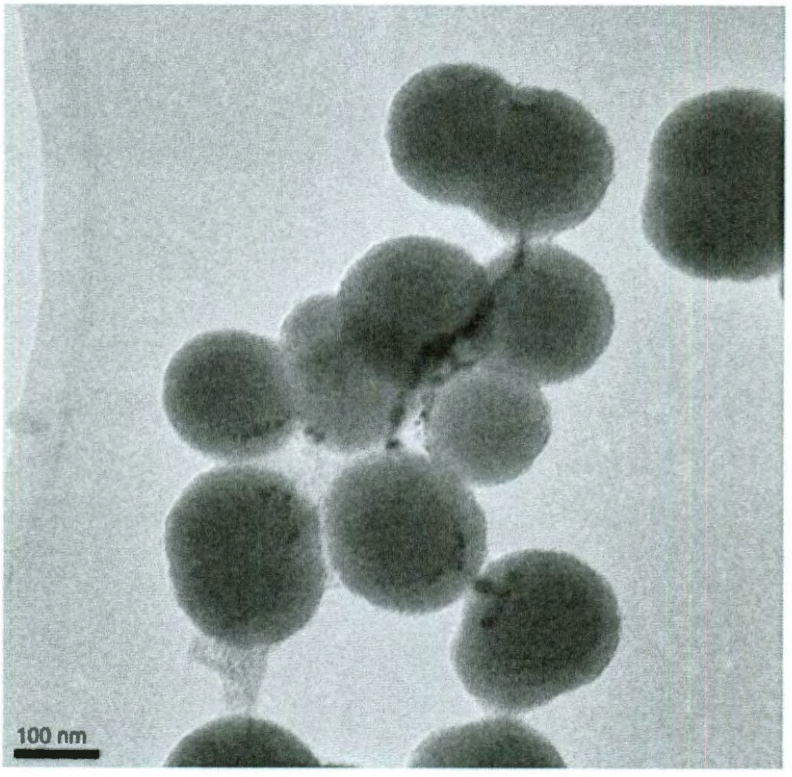


**Figure 1.17.** TEM image of $Si@SiO_2$ particles synthesized with DTAB for 24 hours.

Coating the quantum dots using only a 6 hour reaction time with DTAB was tested. Figure 1.18 is a TEM image of the silica coated synthesized silicon quantum dots from that synthesis. The coating on these particles is much thinner at an average of 60 nm in diameter with some particles at only 40 nm in diameter.

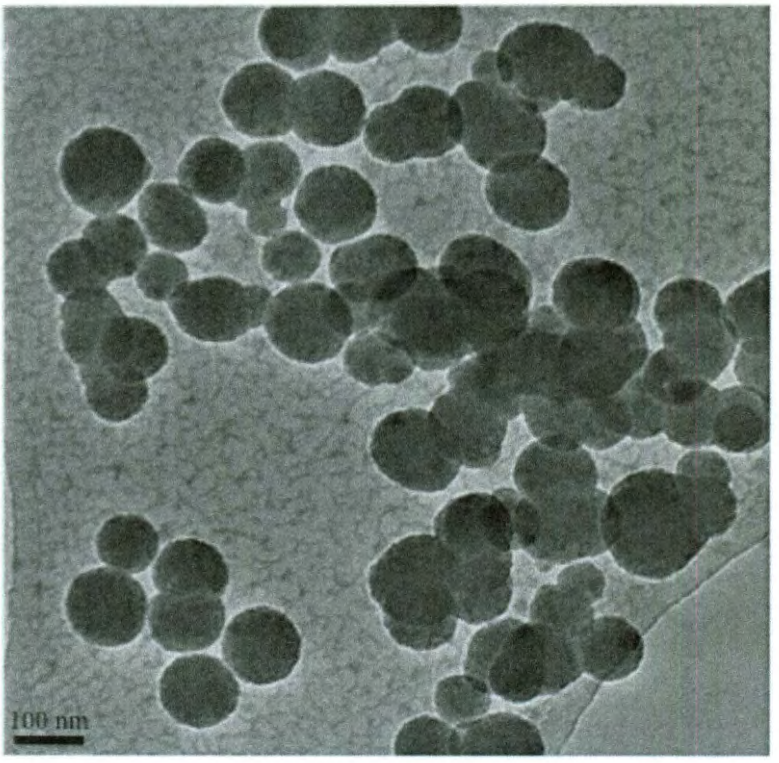


**Figure 1.18.** TEM image of $Si@SiO_2$ particles synthesized using DTAB and a 6 hr reaction time.

After the synthesized Si QDs were coated, the commercial Si QDs were put through the same process to determine whether this coating would work for all quantum dots. Figure 1.19 is a TEM image of the coated commercial silicon quantum dots prepared with DTAB for 6 hours. These particles did not coat individually. Part of the reason for the poor coating may be due to the fact that these particles do not have an electronegative capping ligand on them as the manufacturer does not indicate that there is

a capping ligand on these quantum dots at all. These particles may also be too dilute to initiate an even coating. Due to the undesired coating of these particles, further experimentation did not occur.

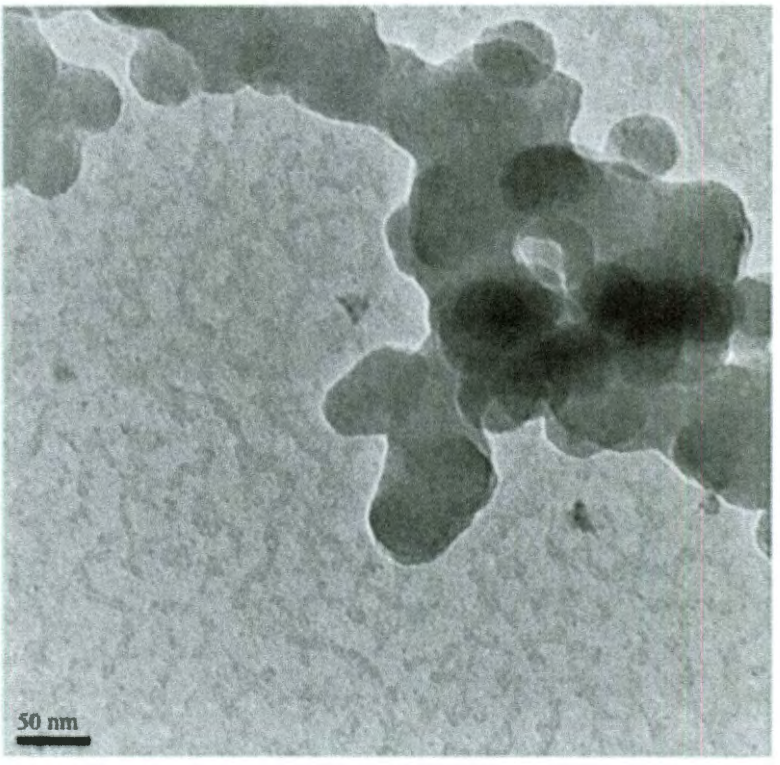


**Figure 1.19.** TEM image of commercial $Si@SiO_2$ particles prepared with DTAB for 6 hrs.

There is one problem with the characterization of the coated silicon particles, and that is that it is difficult to determine the location of the quantum dot. This is because the quantum dot is silicon, and it is coated in a material made primarily of silicon, so analyzing these particles with XPS or HRTEM would not yield any conclusive results. Using a higher density quantum dot would allow for the characterization of the silica coated material with the help of these analytical methods.

**Silica coated germanium quantum dots.** If the quantum dots are made of germanium, XPS and HRTEM should be able to indicate the presence of the quantum dots in the silica so there is evidence that these particles are not just pure silica (Figure 1.20). Germanium has very similar properties compared with silicon, so a quantum dot made of Ge prepared in the same fashion as Si should behave similarly.

For the next set of experiments, DTAB was added to the solution to synthesize spherical particles with six hours of reaction time, and germanium quantum dots were used instead of silicon because this method was already determined to be the most efficient coating method for the Si QDs. Figure 1.21 is an HRTEM image of a Ge@$SiO_2$

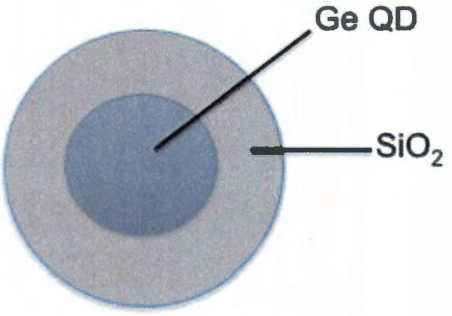


**Figure 1.20.** Theoretical schematic of a silica coated germanium quantum dot.

particle synthesized with DTAB for 6 hours; the Ge quantum dot can be clearly seen in the middle of the silica particle although it is not centered.

The quantum dot can be seen as 10.8 nm away from the edge of the silica in parts and 20.8 nm away from other edges of the silica. Figure 1.22 Shows another HRTEM image of the coated Ge QDs from the same synthesis as above, but multiple quantum dots can be seen in one silica particle. The quantum dots are also at the edges and hardly in the middle of the particle, but this image shows that the quantum dots are an average of 9.8

±4.7 nm apart form each other, which was the goal of the project for electron transfer facilitation.

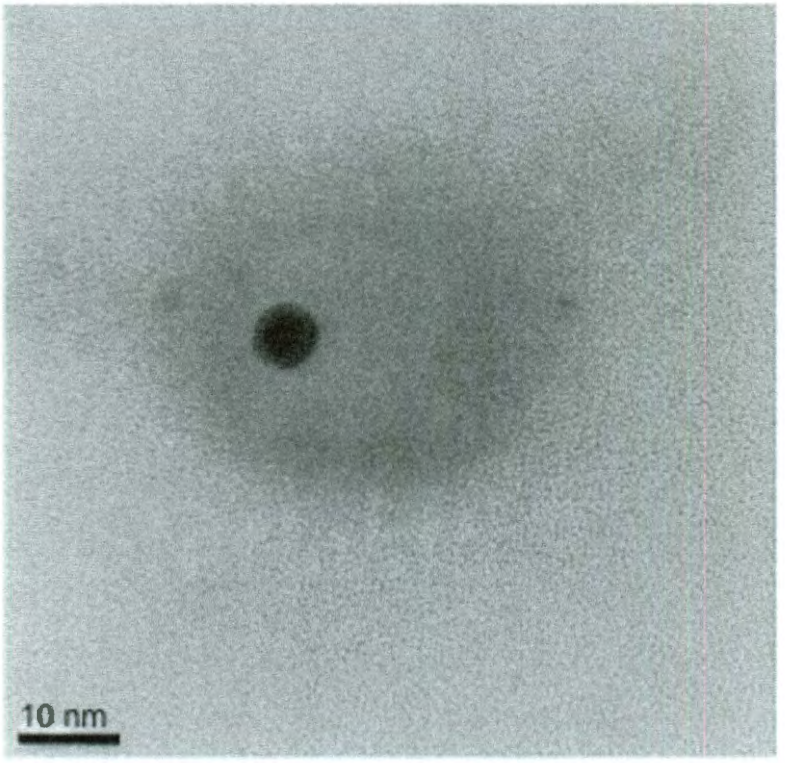


**Figure 1.21**. HRTEM image of $Ge@SiO_2$ particle synthesized with DTAB for 6 hours.

After these particles were determined to coat well, the same process was attempted for the commercial Ge QDs. Figure 1.23 is a TEM image of the coated commercial Ge QDs prepared with DTAB for 6 hours. As observed in the TEM image, the coating of these particles is very similar to that of the commercial Si QDs. This could mean that neither of these particles has a capping ligand, but also these quantum dots in particular are very dilute as indicated by the UV-vis absorbance spectrum. For any further experimentation, these coated particles are not be of use, but the coated synthesized quantum dots are used.

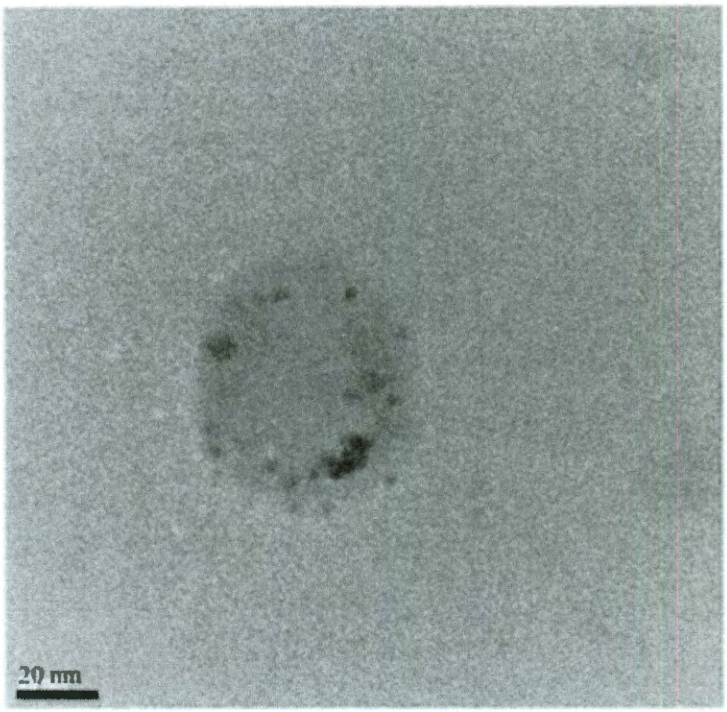


**Figure 1.22.** HRTEM image of $Ge@SiO_2$ particle synthesized with DTAB for 6 hours.

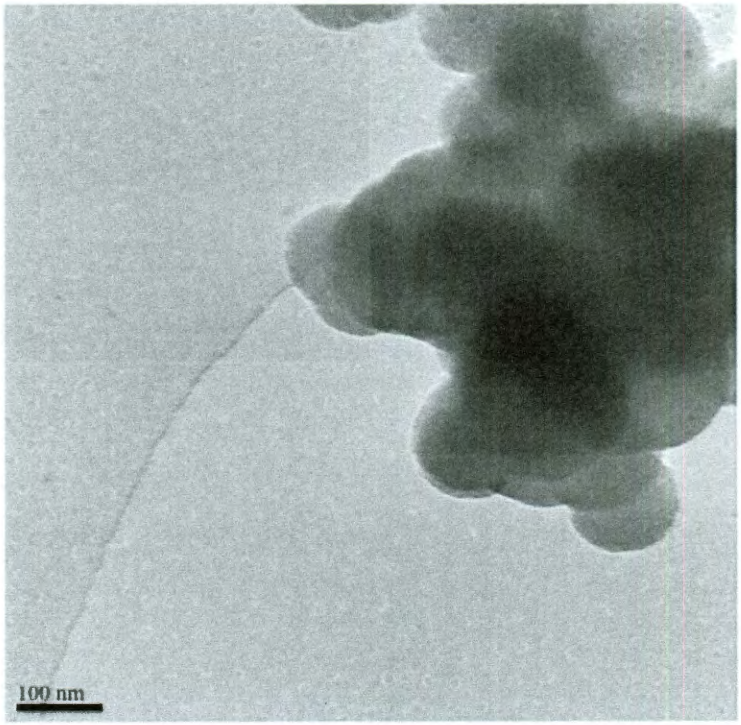


**Figure 1.23.** TEM image of commercial $Ge@SiO_2$ particles prepared with DTAB for 6 hrs.

XPS data was also collected on the $Ge@SiO_2$ particles to determine if germanium is present in the particles. Figure 1.24 shows the survey scans of the coated nanoparticles. The indium peaks are from the indium foil substrate on which the particles are dried. There is a carbon peak in the scan that is visible; this is more than likely not from DTAB even though it was used as a surfactant because bromine and nitrogen peaks are not seen in the scan (Figure 1.16, DTAB).

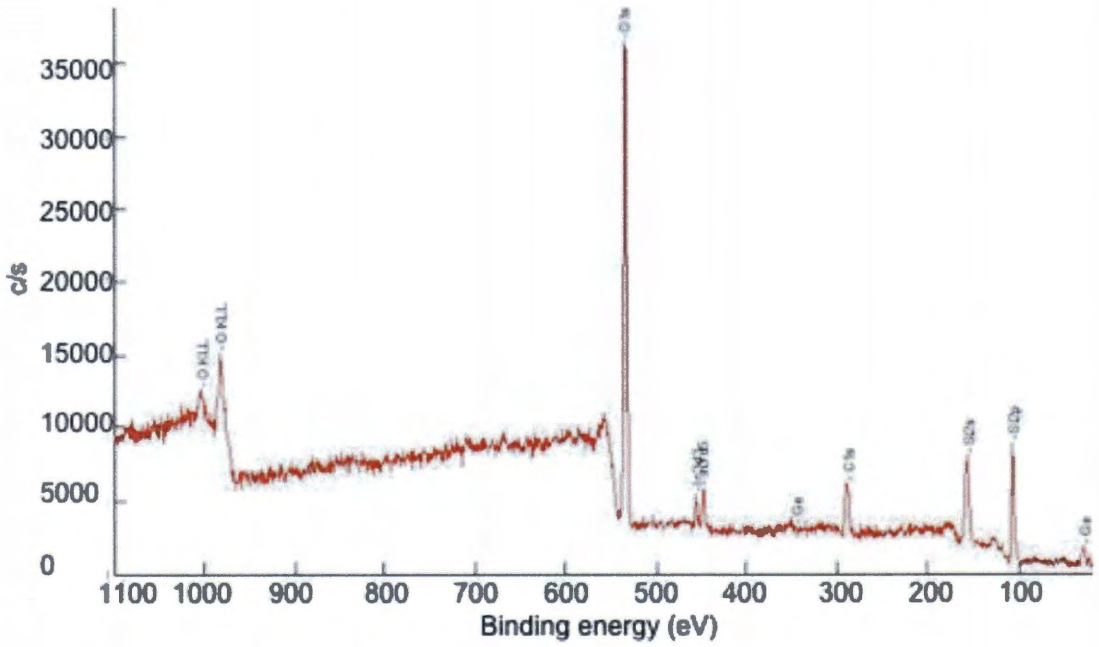


**Figure 1.24.** XPS survey scan of $Ge@SiO_2$ particles.

A closer look at the high resolution silicon and germanium peaks reveals the true nature of the material in these nanoparticles (Figure 1.25). Table 1.2 contains the peak identifications for the silicon and germanium peaks. The silicon peak is characteristic of Si 2p which has a $SiO_2$ electronic environment and a Si-O electronic environment present. The Ge 3d peak is characteristic germanium which reveals that there is a Ge-O

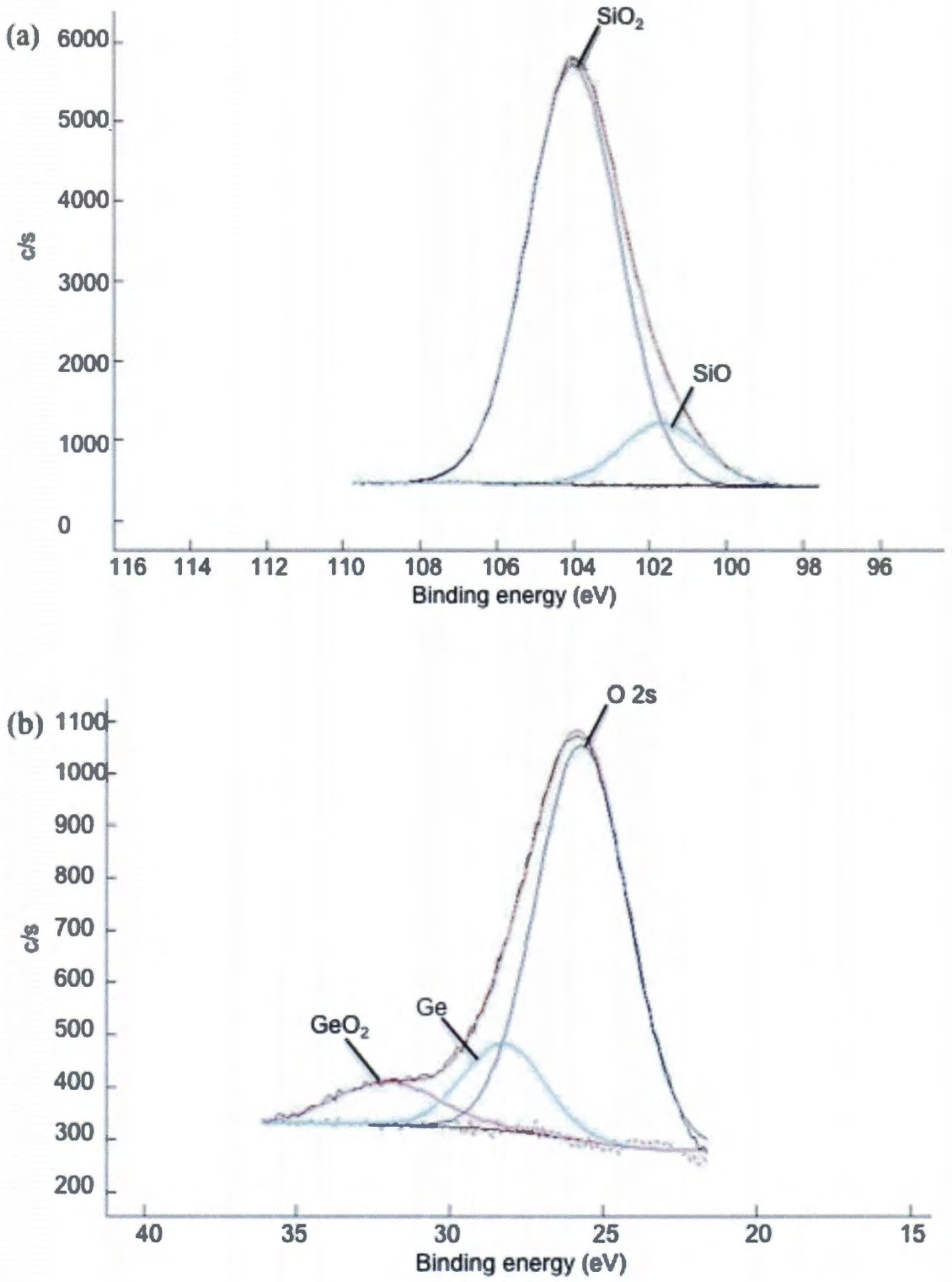


**Figure 1.25.** High resolution XPS data of peak of (a) Si 2s and (b) Ge 3d of Ge@$SiO_2$ particles.

electronic environment as well as elemental Ge. The Ge-O would be present between the quantum dot and the silica, and the elemental Ge would be in the quantum dot. There is another peak that overlaps with the germanium peak, which corresponds to a 2s oxygen with an electronic environment that more than likely corresponds to the oxygen in silica.[18]

**Table 1.2.** XPS peak energy identification.

| Peak | Identification |
|---|---|
| Si 2p - 104.0 eV | $SiO_2$ |
| Si 2p - 101.7 eV | SiO |
| Ge 3d - 32.4 eV | Ge |
| Ge 3d - 28.2 eV | $GeO_2$ |
| O 2s - 25.7 eV | $SiO_2$[18] |

The XPS data does confirm the TEM image which shows many quantum dots on or near the surface and deeper inside of the particles as well. From this data it is assumed that there is an even mixture of particles which have quantum dots in the center and on the outer edges of the silica.

## Conclusions

Silicon or germanium quantum dots were successfully synthesized using a bottom up method verified with UV-vis and AFM images. Silica coatings were produced using an LPD method with and without a surfactant. The coating thickness could be controlled with reaction duration and DTAB as a surfactant. Using germanium quantum dots, the

location of the quantum dots in the silica matrix could be determined with the help of HRTEM and XPS. The spacing of the quantum dots was determined to be in the appropriate range (10 nm) for further experimentation.

## Experimental

**General.** All chemicals were obtained commercially and most were used without further purification with the exception of solvents. For the quantum dot synthesis, tetraoctylammonium bromide (TOAB), silicon tetrachloride (99.998%), lithium aluminum hydride (1.0M in tetrahydrofuran), methanol (≥99.8%), hexachloroplatinic acid hydrate (≥99.9%), isopropanol (≥99.5%), and allylamine (99+%) were obtained from Sigma Aldrich; toluene was obtained from EMD and germanium tetrachloride (99.99%) was obtained from Acros Organics. Methanol, toluene, and isopropanol were further purified of dissolved oxygen using a freeze-pump-thaw method. For the silica coating, fumed silica (99.8%), hexafluorosilicic acid (34%), and dodecyltrimethylammonium bromide (99%) were obtained from Sigma Aldrich; ethanol (200 proof) was obtained from Decon Laboratories. Silicon nanocrystals (5 nm) stored in acetonitrile and germanium nanocrystals (20 nm) stored in methanol were obtained from Universal Nanotech Corporation.

Characterization of these materials were performed with a JEOL 2010 transmission electron microscope (TEM) at 100 kV with a CCD camera. High resolution transmission electron microscopy was performed on a JEOL 2100 field emission gun TEM at 200 kV with a CCD camera. Atomic force microscopy (AFM) was performed on a Digital Image Nanoscope IIIA in tapping mode. UV-visible spectroscopy was performed on an Agilent 8453 UV-visible spectroscopy system with 1 cm quartz cuvettes. X-ray photoelectron spectroscopy (XPS) was performed on a PHI Quantera X-ray photoelectron spectrometer equipped with a differential argon ion gun with indium foil as a substrate for the samples.

**Silicon quantum dots**. The entire synthesis of the quantum dots was performed in a glove box under a controlled nitrogen atmosphere to ensure no oxygen was present. All solvents in this synthesis were made anhydrous using a freeze-pump-thaw method. The quantum dots were synthesized in anhydrous toluene (100 mL) with tetraoctylammonium bromide (TOAB) (1.5 g, 2.7 mmol) used as a surfactant and $SiCl_4$ (92 μL, 0.8 mmol). The solution was stirred vigorously for 24 hours to ensure that the reverse micelles formed completely and uniformly. $LiAlH_4$ in THF (0.63 μL, 1.0 M) was added to this solution as a reducing agent, and the solution was allowed to react for 3 hours while continuously being stirred vigorously. The excess $LiAlH_4$ was quenched using anhydrous MeOH (15 mL). The quantum dots are hydrophobic at this point, but they need to be hydrophilic for further experimentation.[3]

To make the particles hydrophilic, $H_2PtCl_6$ in anhydrous isopropanol (40 μL, 0.05 M) was added to the quantum dots along with allylamine (2 mL, 26.7 mmol); this mixture was allowed to react until the solution stopped producing hydrogen gas. This solution is air stable and was taken out of the glove box to evaporate off the liquid, but heat was not added to the system because the quantum dots easily oxidize to silica with added energy. After drying, the particles were resuspended in deionized water (35 mL) and filtered through a 0.2 μm pore filter to remove any excess surfactant leaving the quantum dots alone in the water.[3]

**Germanium quantum dots**. The entire synthesis of the quantum dots was performed in a glove box under a controlled nitrogen atmosphere to ensure no oxygen was present. All solvents in this synthesis were made anhydrous using a freeze-pump-thaw method. The quantum dots were synthesized in anhydrous toluene (100 mL) with tetraoctylammonium bromide (TOAB) (1.5 g, 2.7 mmol) used as a surfactant and $GeCl_4$ (92 μL, 0.8 mmol). The solution was stirred vigorously for 24 hours to ensure that the reverse micelles formed completely and uniformly. $LiAlH_4$ in THF (0.63 μL, 1.0 M) was

added to this solution as a reducing agent, and the solution was allowed to react for 3 hours while continuously being stirred vigorously. The excess $LiAlH_4$ was quenched using anhydrous MeOH (15 mL). The quantum dots are hydrophobic at this point, but they need to be hydrophilic for further experimentation.[3]

To make the particles hydrophilic, $H_2PtCl_6$ in anhydrous isopropanol (40 μL, 0.05 M) was added to the quantum dots along with allylamine (2 mL, 26.7 mmol); this mixture was allowed to react until the solution stopped producing hydrogen gas. This solution is air stable and was taken out of the glove box to evaporate off the liquid, but heat was not added to the system because the quantum dots easily oxidize to silica with added energy. After drying, the particles were resuspended in deionized water (35 mL) and filtered through a 0.2 μm pore filter to remove any excess surfactant leaving the quantum dots alone in the water.[3]

**Silica coated Si QDs**. Prior to coating the quantum dots, an $H_2SiF_6$ precursor solution was saturated with $SiO_2$ to ensure the highest concentration of $H_2SiF_6$; this solution was saturated by adding fumed silica (3 g) to $H_2SiF_6$ (50 mL). The mixture was stirred vigorously for 24 hours and filtered through a 0.2 μm pore vacuum filter.[14-16] The coating is done with a liquid phase deposition method, and the quantum dots are used to seed the silica growth. The quantum dots were coated by vigorously stirring Si QD solution (10 mL), DTAB in deionized water (13.4 mL, 0.117 M), and saturated $H_2SiF_6$ solution (6.6 mL) in a plastic centrifuge tube due to the HF byproduct. This solution was stirred and heated to 30 °C for 6 - 24 hours depending on the desired thickness. After the reaction was complete, the solution was centrifuged and washed with EtOH (10 mL) many times to ensure all of the HF byproduct was removed.[14-16]

**Silica coated Ge QDs**. Prior to coating the quantum dots, an $H_2SiF_6$ precursor solution was saturated with $SiO_2$ to ensure the highest concentration of $H_2SiF_6$; this

solution was saturated by adding fumed silica (3 g) to $H_2SiF_6$ (50 mL). The mixture was stirred vigorously for 24 hours and filtered through a 0.2 μm pore vacuum filter.[14-16] The coating is done with a liquid phase deposition method, and the quantum dots are used to seed the silica growth. The quantum dots were coated by vigorously stirring Ge QDs solution (10 mL), DTAB in deionized water (13.4 mL, 0.117 M), and saturated $H_2SiF_6$ solution (6.6 mL) in a plastic centrifuge tube due to the HF byproduct. This solution was stirred and heated to 30 °C for 6 - 24 hours depending on the desired thickness. After the reaction was complete, the solution was centrifuged and washed with EtOH (10 mL) many times to ensure all of the HF byproduct was removed.[14-16]

## References


1. T. Soga, *Nanostructured Materials for Solar Energy Conversion,* Elsevier, New York, 2006.
2. H. S. Mansur, *WIREs Nanomed. Nanobiotechnol.*, 2010, **2**, 113.
3. J. H. Warner, A. Hoshino, K. Yamamoto, and R. D. Tilley, *Angew. Chem., Int. Ed.,* 2005, **44**, 4550.
4. E.-C. Cho, M. A. Green, G. Conibeer, D. Song, Y.-H. Cho, G. Scardera, S. Huang, S. Park, X. J. Hao, Y. Huang, and L. V. Dao, *Adv. OptoElectron.,* 2007, **69578**, 1.
5. A. R. Barron, C. E. Hamilton, and C. Smith, *Chemistry of the Main Group Elements,* Connexions web site, http://cnx.org/content/col11124/1.25/.
6. S. Baskoutas, V. Kapaklis, and W. Schommers, *J. Nanosci. Nanotechnol.,* 2006, **6**, 2037.
7. J. Singh, *Semiconductor Devices: Basic Principles*, John Wiley, New York, 2001.
8. H. Takagi, H. Ogawa, Y. Yamazaki, A. Ishizaki, and T. Nakagiri, *Appl. Phys. Lett.,* 1990, **56**, 2379.

9. S. Prabakar, A. Shiohara, S. Hanada, K. Fujioka, K. Yamamoto, and R. D. Tilley, *Chem. Mater.,* 2010, **22**, 482.

10. M. V. Wolkin, J. Jorne, and P. M. Fauchet, *Phys. Rev. Lett,.* 1999, **82**, 197.

11. T. H. DiStefano and D. E. Eastman, *Solid State Commun.,* 1971, **9**, 2259.

12. M. Yamamoto, K. Hayashi, K. Tsunetomo, K. Khono, and Y. Saka, *J. Appl. Phys.,* 1991, **30**, 136.

13. W. A. Saunders, P. C. Sercel, R. B. Lee, H. Atwater, K. J. Vahala, R. C. Flanagan, and E. J. Escorsi-Aparcio, *Appl. Phys. Lett.,* 1993, **63**, 1549.

14. E. A. Whitsitt, Ph.D. thesis, Rice University, 2004.

15. E. A. Whitsitt and A. R. Barron, *Chem. Commun.,* 2003, **9**, 1042.

16. E. A. Whitsitt and A. R. Barron, *J. Colloid Interf. Sci.,* 2005, **287**, 318.

17. A. Orbaek, M. McHale, and A. R. Barron, *Silver Nanoparticles: A Case Study in Cutting Edge Research*, Connexions web site, http://cnx.org/content/m19597/1.11.

18. NIST web site, http://srdata.nist.gov/xps/Default.aspx.

# Chapter 2
# Array of Coated Quantum Dots

## Introduction

Colloidal crystals are three-dimensional assemblies of monodispersed silica or polystyrene spheres.[1] These assemblies have become an interest for applications in anti-reflective coatings, optical filters, and solar cells.[2] There are many methods to produce colloidal crystals, such as: gravity sedimentation, electrophoretic deposition, spin coating, centrifugation, capillary deposition, and vertical deposition.[3-11] Gravity sedimentation takes weeks to do on the small scale, so using that method for mass production would be very time consuming and difficult.[3] Electrophoretic deposition, spin coating, centrifugation, and capillary deposition would add some cost to production, and most of these methods would be very difficult to incorporate into mass production on a large scale.[4-7] For the best control, the vertical deposition method of assembly appears to have the most success because it is the most reproducible and reliable method of the above mentioned; this method also would be easiest to add to current solar cell fabrication with little additional cost and no additional instrumentation because it does not require special equipment or environment to produce the array.[8-11]

For this part of the project, the silica coated quantum dots will be used to make the assembly. Using these particles will allow for a similar approach as that reported in literature since the particles are externally silica. There are several conflicting results published, which indicate ethanol only or water only or a mixture of the two as the best solvent for assembly control.[9-11] The solvent could then be tuned to determine the optimal solvent for the assembly of silica coated quantum dots. Arraying these particles will facilitate electron transfer between particles with illumination for good conductivity and little energy loss. As mentioned in previous chapters, the quantum dots are required to be no more than 10 nm apart from each other, and arraying them is the most efficient way to

ensure the particles are close enough together. This array would be used as a tandem cell to the terrestrial first generation silicon solar cell to increase efficiency without raising production costs too much or requiring new manufacturing facilities.

## Results and Discussion

The arrays were made by a vertical deposition method. The coated quantum dots were put in a solvent (water, ethanol, or a mix of the two) with a slide standing vertically, and the solution was evaporated on its own time at room temperature. This technique allows the particles to align themselves at the solvent surface on the slide using the meniscus as a guide (Figure 2.1).

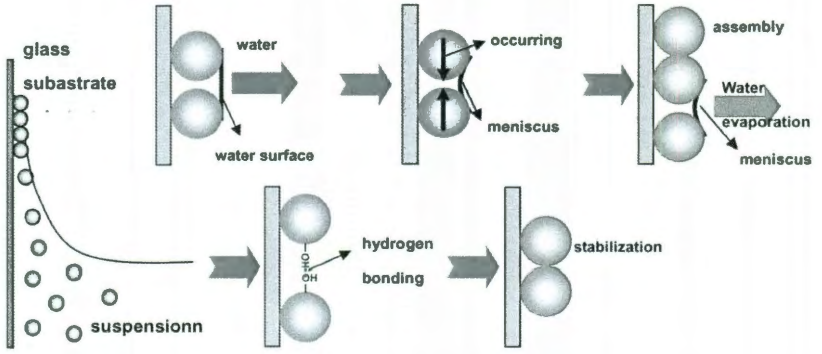


**Figure 2.1.** Schematic of vertical deposition technique (Adapted from T.H. Kim, T. S. Lee, and W. S. Lyoo, *Mol. Cryst. Liq. Cryst.*, 2007, **464**, 153).

Extensive research has been done on making arrays, and one group proposed that using a 1:3 (v:v) EtOH:$H_2O$ mixture produces the best array,[10,11] so this solvent mixture was tested first (Figure 2.2). This array took 36 hours to form and dry. From the SEM images, there are parts of this slide that are seen as arrayed, but most of the material is not organized in any way. The ridge seen in the middle of Figure 2.2a is from sonication, so part of the problem with forming this array is settlement because after the solution was

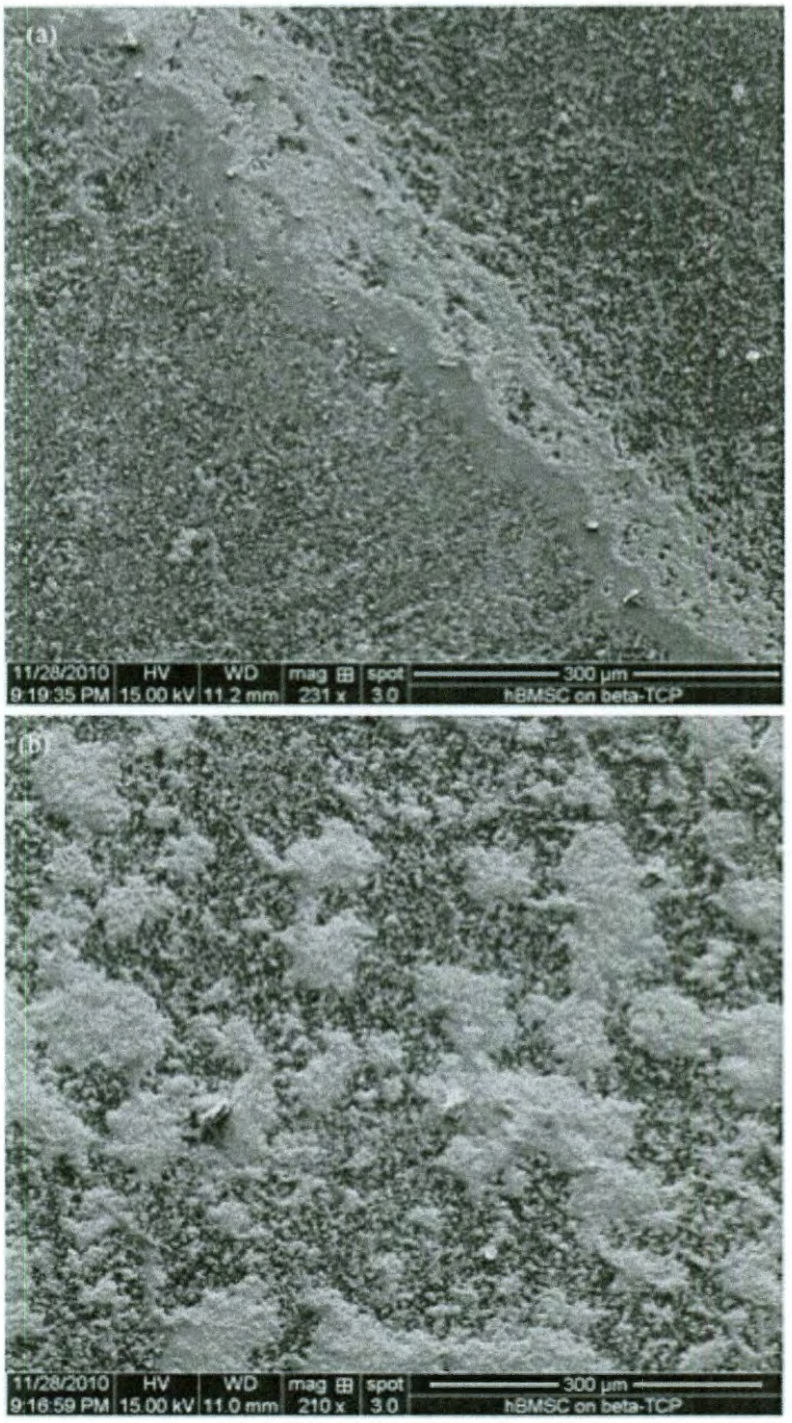


**Figure 2.2**. SEM images of an array of 1:3 (v:v) EtOH:$H_2O$ Si@$SiO_2$ particles (a) broad view of sample and (b) close up of particles.

sonicated and more particles were ensured to be in solution, a ridge of closer packed particles formed.

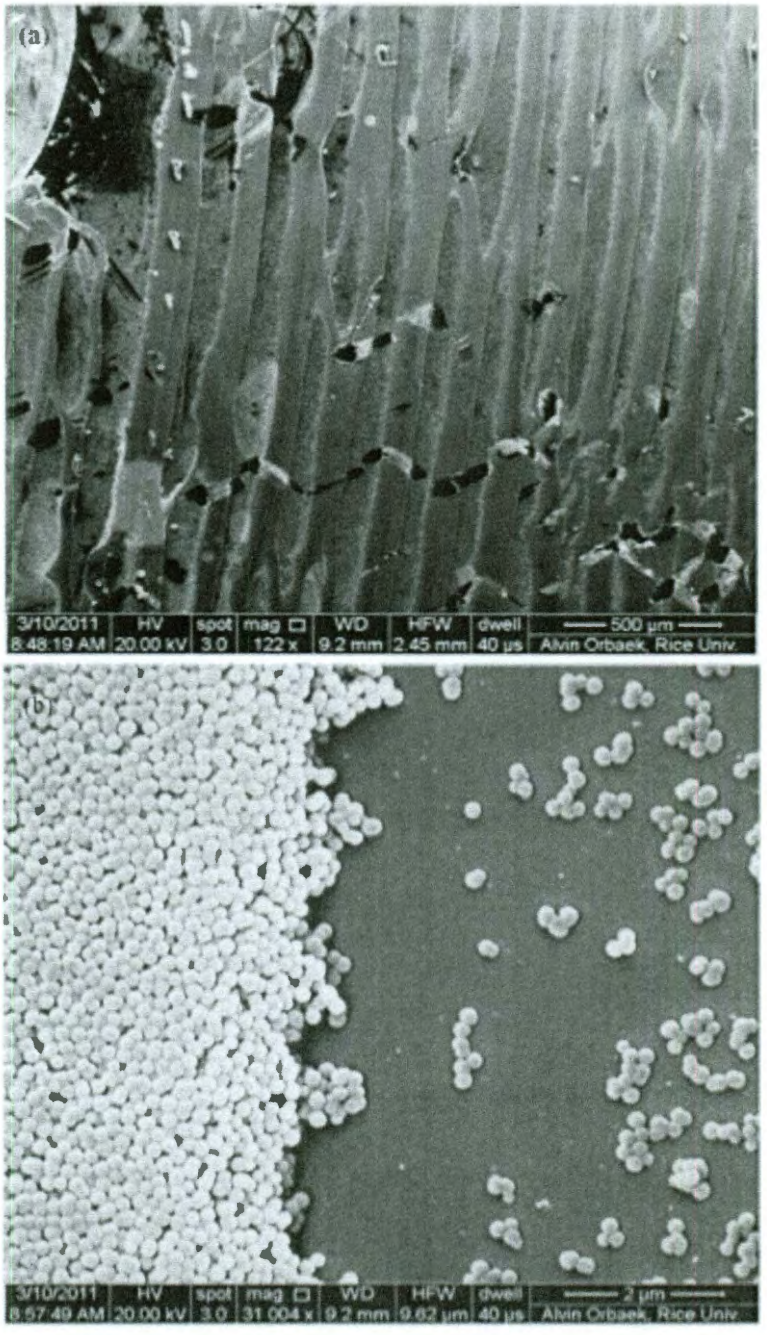


**Figure 2.3**. SEM images of pure EtOH of $Si@SiO_2$ particles (a) broad view of sample and (b) close up of particles.

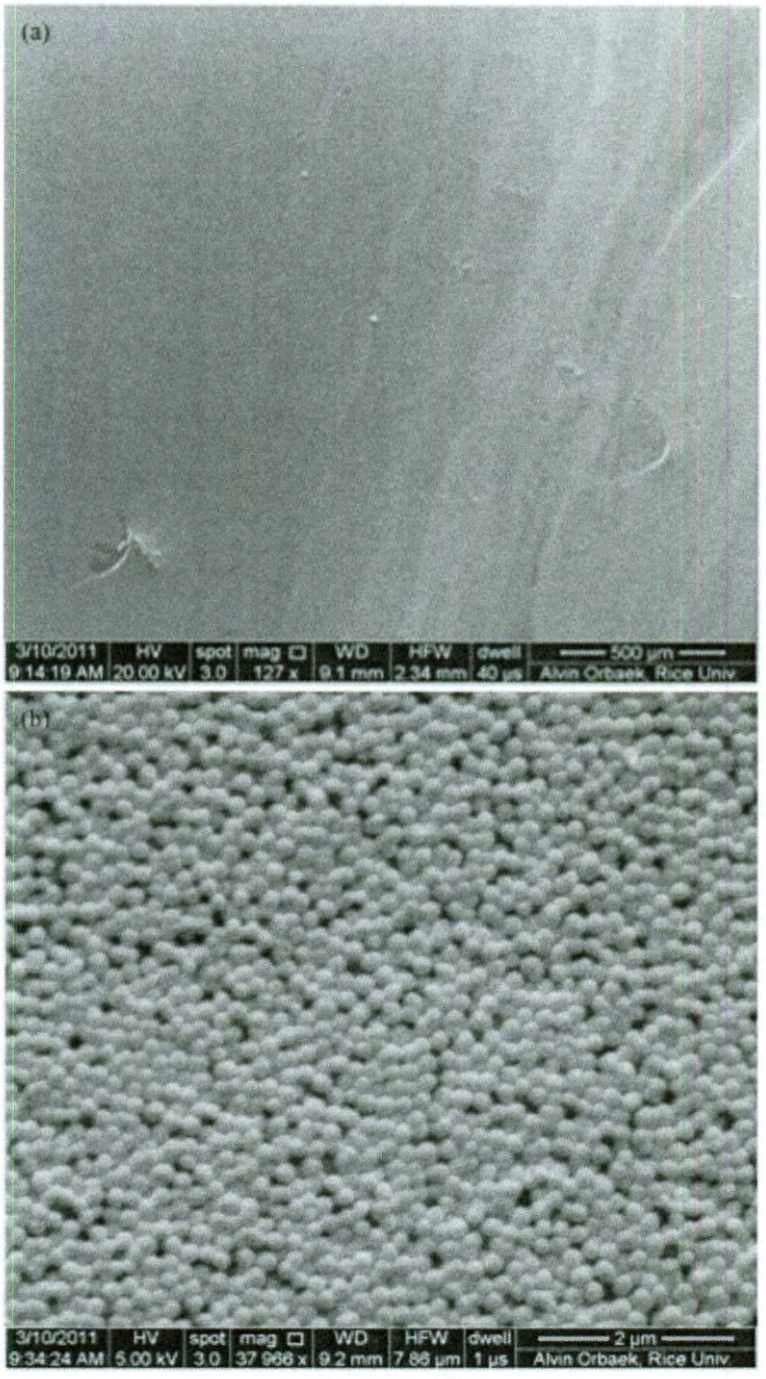


**Figure 2.4.** SEM images of $Si@SiO_2$ particles in deionized $H_2O$ (a) broad view of sample and (b) close up of particles. Average particle size: 150 nm. Average particle distance: 170 ±30 nm.

Other research has indicated that pure water or pure ethanol will be more efficient with arraying the particles.[8-10] Pure ethanol was tested next. The ethanol evaporated too quickly to sonicate, so the particles remained suspended the entire time. This deposition took only a few hours (6 - 12), and even with the particles staying suspended, there remain areas of the slide, which are not covered in particles (Figure 2.3). There appears to be waves of arrayed and random particle placement. Since these arrays were made in a fume hood, the changing flow of the hood created periods where the ethanol evaporated slowly enough to array the particles and then too quickly for the particles to place. From these SEM images, it is obvious that ethanol is not an ideal solvent for arraying these particles due to the inconsistency of the deposition.

Changing the solvent from pure ethanol to deionized water only, a much more uniform array can be seen (Figure 2.4). Larger particles (150 nm) were used for the arrays so that the SEM could show each individual particle. Image in Figure 2.4a shows a broad view of the array, image (b) is a close up of the individual particles. From image in Figure 2.4b, it is obvious that all of the particles are not close packed, but close packing is not necessary. To have the particles close packed would yield the best efficiency, but as long as the particles are touching for the most part, there will still be electronic transfer. The center of the particles are 170 ±30 nm apart from each other, which means that there is some close packing with the particles being only 150 nm to begin with. This array solution was sonicated every few hours to ensure the particles did not fall out of solution, and the deposition took 48 hours to complete. Based on these results, deionized water only will be used for the rest of the arrays.

**Thickness control.** Since a successful array was created, thickness control needed to be determined. A solution with the usual amount of material, calculated assuming 100% product yield and no product loss between washes, with a concentration of 1.8 M;

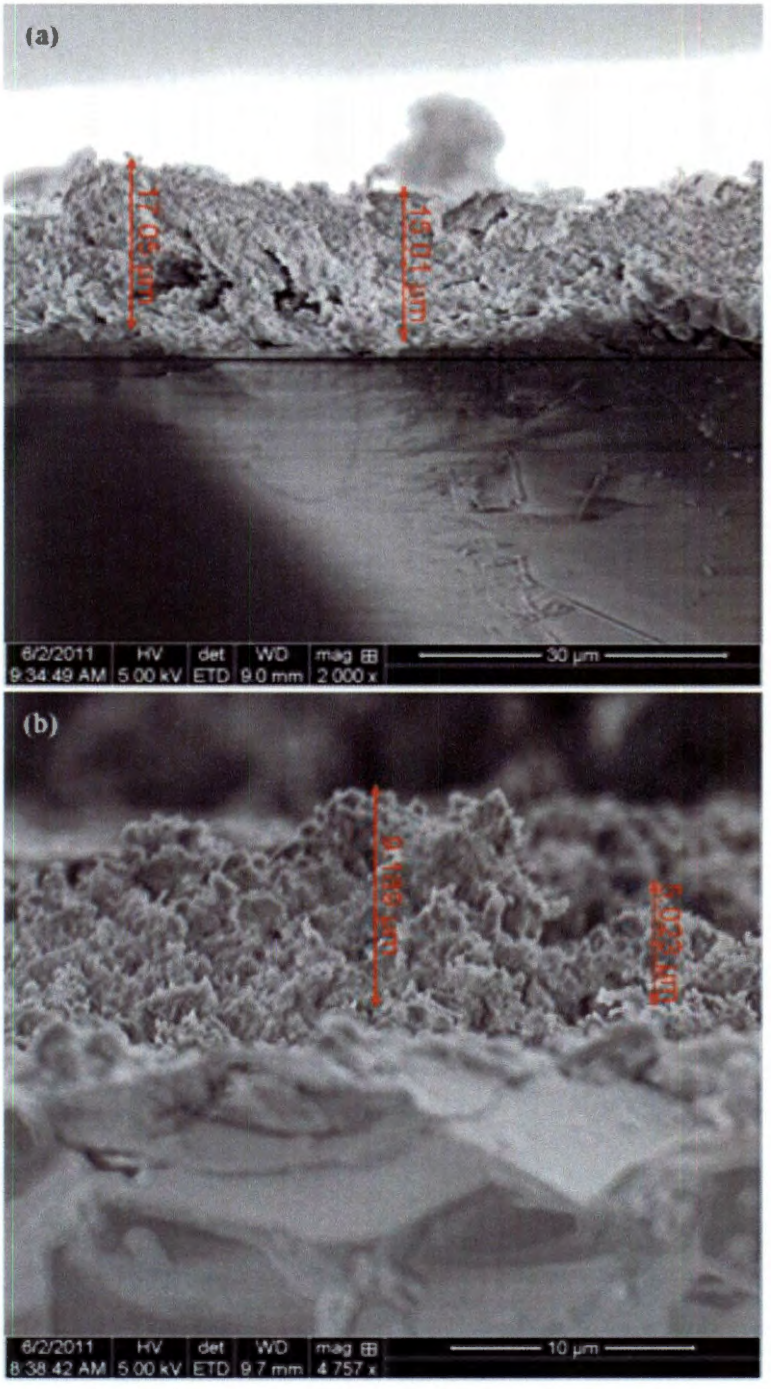


**Figure 2.5.** Cross-sectional SEM images of (a) 1.8 M and (b) 0.9 M of $Si@SiO_2$ particles.

and a solution with half of the material, with a concentration of 0.9 M, diluted in water were arrayed to determine if half of the material was used it would yield an array with

half the thickness. Cross-sectional SEM images of silica coated silicon arrays show that thickness of the array can be controlled with amount of material in solution (Figure 2.5). The 1.8 M array has a thickness of about 16.4 μm, whereas the 0.9 M array has a thickness of about 7.5 μm. The coating thickness of the 0.9 M array is nearly half the thickness of the 1.8 M array, which shows thickness control with sample amount. However, the array made with 0.9 M solution of particles is not nearly as uniform in thickness across the sample as the 1.8 M array. UV-visible absorbance was also taken of these arrays to determine if absorbance changes with array thickness (Figure 2.6). To compare the absorbance of these coatings with a silica control, Stöber particles were synthesized (230 nm) and arrayed in the same manner as the coated quantum dots. The silica control absorbs more than the 0.9 M array of $Si@SiO_2$ particles, but the amount of material used for the silica control was comparable to the 1.4 M array.

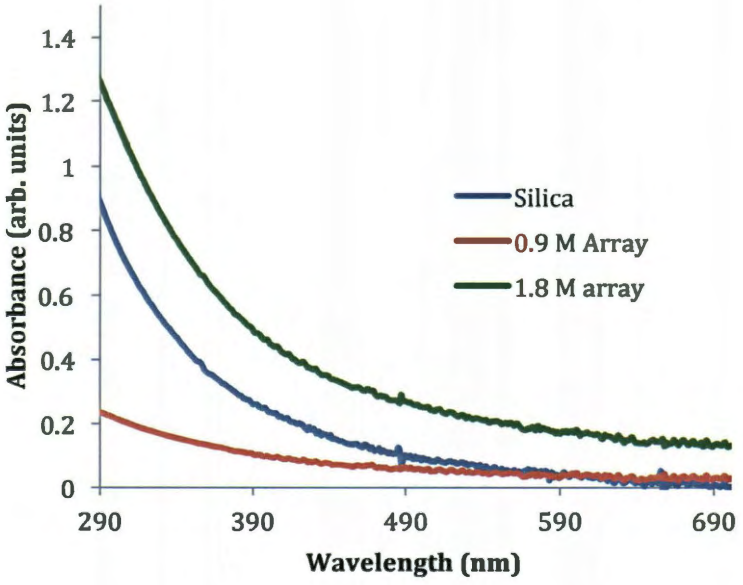


**Figure 2.6.** UV-visible spectra of array thicknesses of $Si@SiO_2$ particles compared to a silica control.

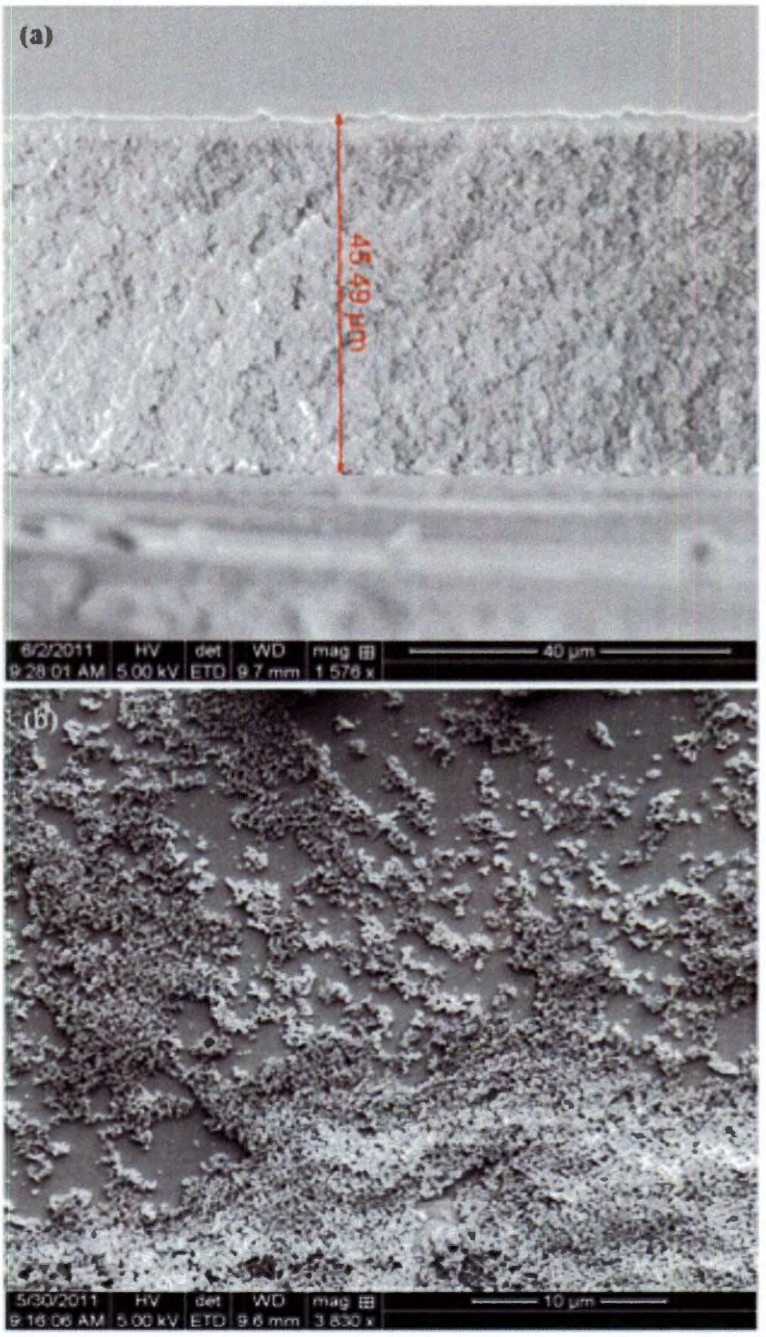


**Figure 2.7.** Cross-sectional SEM image of Ge@$SiO_2$ particles (a) 1.8 M and (b) surface SEM image of 0.9 M.

Silica coated germanium particles were also tested for thickness control. Cross-sectional and surface SEM images (Figure 2.7) of the 1.8 M solution versus the 0.9 M

solution shows that there is much less control with these particles. The 1.8 M solution produces a very nice uniform array of 45.5 μm thick across the entire sample, but less material does not array at all. UV-visible absorbance was taken of the Ge@$SiO_2$ particles arrays as well (Figure 2.8). The coated germanium particles absorb much more than the coated silicon particles, and they absorb more strongly than the silica control even though the array made with the 0.9 M solution did not make a complete array.

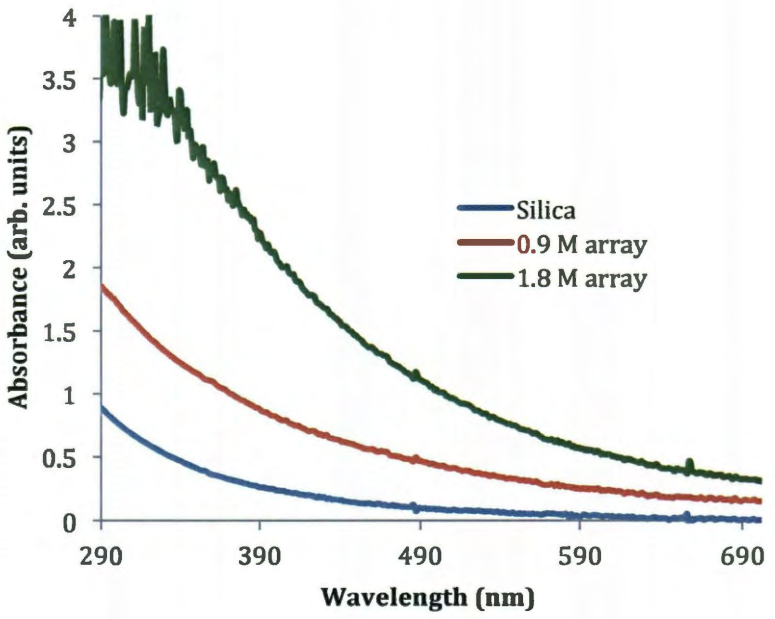


**Figure 2.8.** UV-visible spectra of array thicknesses of Ge@$SiO_2$ particles compared to a silica control.

An EDS elemental map was taken of the silica coated germanium particles to determine if both silicon and germanium can be detected in the array (Figure 2.9). Both elements can be observed with EDS in the array, which means that the quantum dots are present in the arrays.

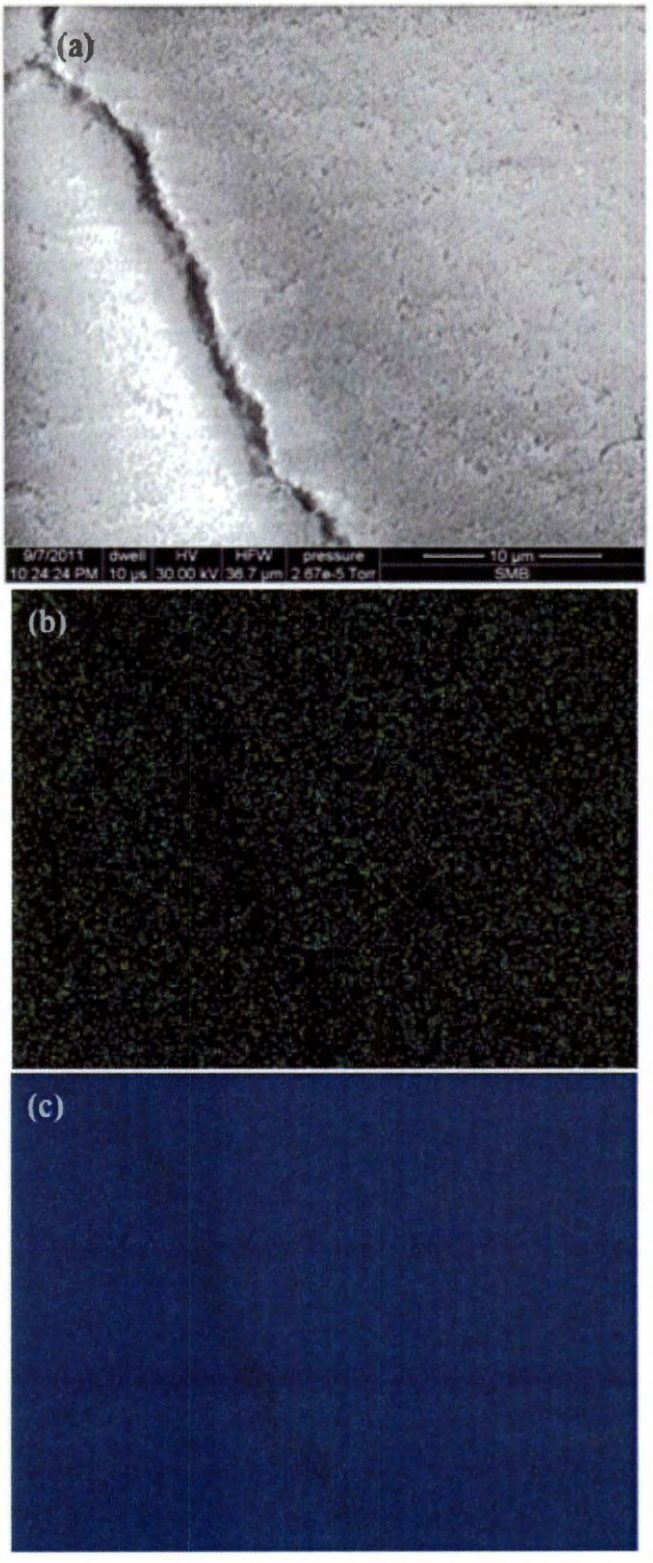


**Figure 2.9.** EDS mapping of (b) germanium and (c) silicon with corresponding (a) SEM image of arrayed Ge@$SiO_2$ particles.

Silica particles were synthesized via a modified Stöber method using tetraethoxysilane (TEOS, Figure 2.10) as the silicon source to produce silica nanoparticles smaller than the typical 300 nm, which the traditional method yields. Figure 2.11a is a TEM image of the silica particles. These particles were then arrayed in water just as the coated quantum dots are arrayed. Figure 2.11 is a picture of the array after it dried. These particles array in strands and tend not to stick to the substrate, which makes the array very delicate and brittle. Only UV-visible absorbance (Figures 2.6 and 2.8) was possible to measure on this array because more handling prompted the silica to fall off; therefore, no SEM image is available for this sample.

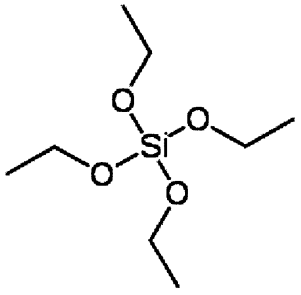


**Figure 2.10.** Structure of tetraethoxysilane (TEOS).

**Photoconductivity.** Photoconductivity testing was done on $Si@SiO_2$ particle and $Ge@SiO_2$ particle arrays. These arrays were made on ITO glass instead of quartz because ITO glass is conductive. UV-visible absorbance was taken of these arrays compared to ITO glass as a control to ensure the material absorbed better than the glass alone (Figure 2.12).

The photoconductivity of the solar cell was crudely tested with white light and with 254 nm UV light. The cell was painted with conductive graphite on part of the slide that was not coated with material and on spots that were coated to make contacts to complete the circuit. Figure 2.13 shows the circuit diagram of the photoconductivity test, and Figure 2.14 shows the cross-sectional view of the test. The power source was a

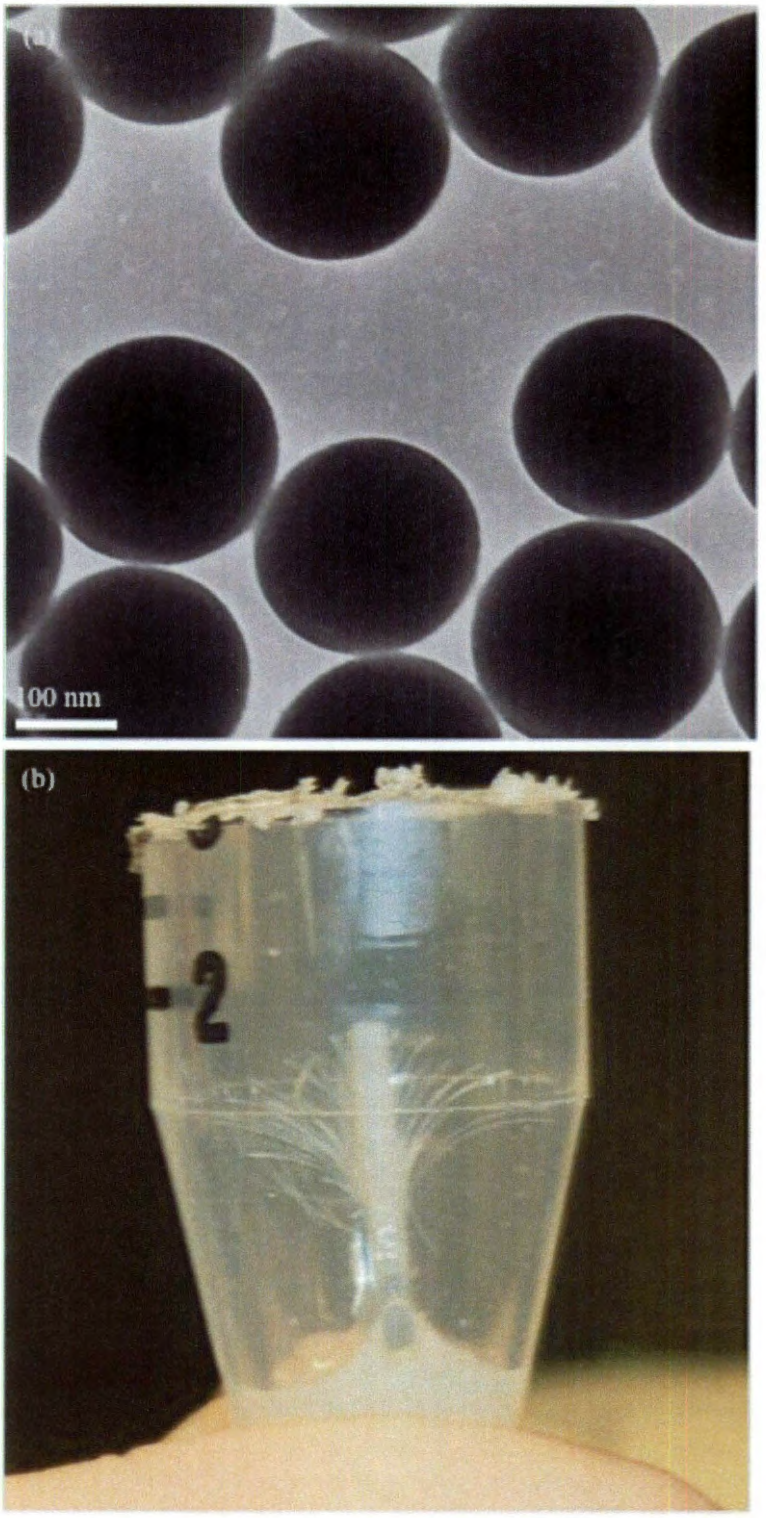


**Figure 2.11.** (a) TEM image of modified Stöber particles and (b) a picture of the array of these particles.

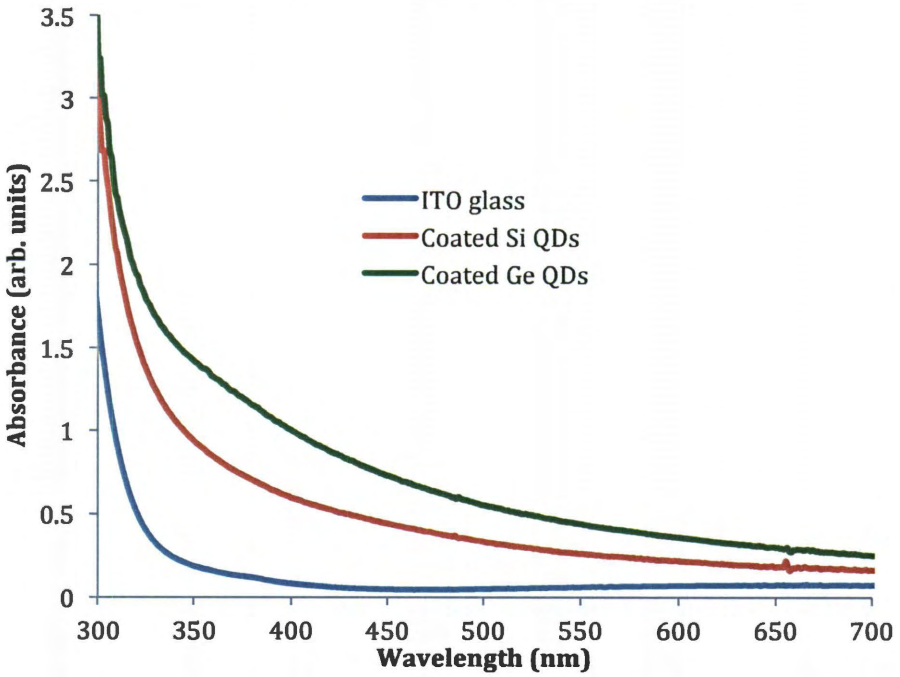


**Figure 2.12.** UV-visible spectra of ITO glass and coated ITO glass with QDs@$SiO_2$.

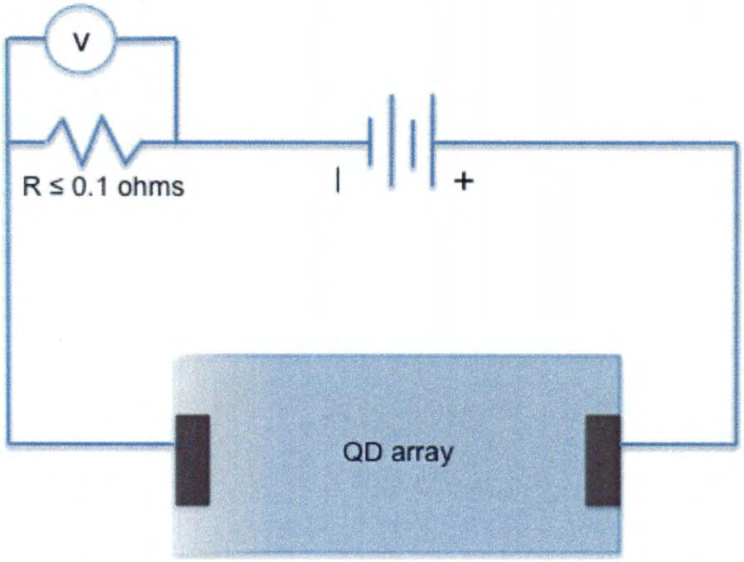


**Figure 2.13.** Circuit diagram of photoconductivity test.

simple 9 V battery. The voltmeter and 0.1 Ω resistor were placed on a breadboard with the cell and battery as the diagram indicates.

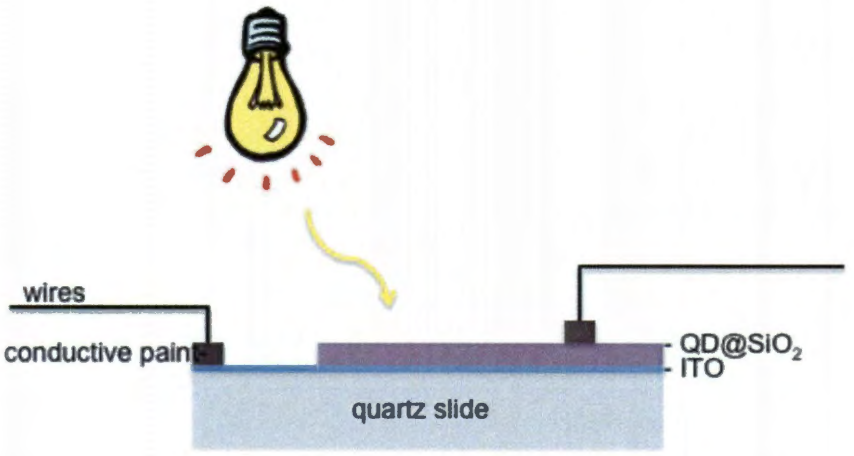


**Figure 2.14.** Cross-sectional view of photoconductivity test on QD array.

The results of the conductivity tests were inconsistent and only gave positive results on certain areas of the cell. With white light, only the Ge@$SiO_2$ cell showed areas of 0.2 mV, which equals 2 mA of photo-current. The Si@$SiO_2$ cell showed no photoconductivity for white light, but this seems reasonable, as the Si QDs do not absorb in the visible part of the spectrum. The photoconductivity with 254 nm UV light was greater for both. The Si@$SiO_2$ cell photoconducted 0.4 mV in UV light, which is equal to 4 mA of current; the Ge@$SiO_2$ cell photoconducted 0.7 mV in UV light, which is equal to 7 mA of current. Although the photoconductivity of the cells was inconsistent, these are positive results suggesting that the cells, with further improvement and optimization, could be completely photoconductive.

## Conclusions

A successful array was produced when the particles were suspended in water only and allowed to assemble with a vertical deposition method. Thickness was controllable for silica coated silicon quantum dots but not for the coated germanium particles. Although inconsistent, the arrays were proven to be photoconductive in areas.

## Experimental

**General.** All materials were obtained commercially and were not further purified. Quartz slides (75 x 25 x 1 mm) were obtained from Chem Glass. Indium tin oxide (ITO) coated glass slides (75 x 25 x 1 mm, 8-12 Ω/sq surface resistivity) came from Sigma Aldrich. Tetraethoxysilane (TEOS) (metals basis) was obtained from Alfa Aesar. Methanol was obtained from Sigma Aldrich, and ammonium hydroxide (14.8 M) came from EMD.

Characterization of the arrays was performed with a FEI Quanta 400 ESEM FEG scanning emission microscope equipped with an EDAX energy dispersive spectroscope. Absorbance was performed on an Agilent 8453 UV-visible spectroscopy system with 1 mm thick quartz or ITO glass slides.

**Array.** To control the array best, a 1 x 1 cm quartz slide or ITO (indium tin oxide) glass slide was placed vertically in a centrifuge tube with the coated QD solution (2 mL) having the slide completely submerged. The solvent of the coated QD solution varied between pure ethanol, an ethanol/water mix, and pure water to determine the optimum packing for the array. The solution with the slide was then set to dry in a fume hood at the solvent's evaporation pace at room temperature. Not increasing the speed of evaporation with heat or vacuum allowed the particles to align themselves at the very top of the meniscus while the solvent dried slowly (Figure 2.1).[8-11] The solution with the slide was sonicated briefly every couple of hours to ensure that the particles were evenly dispersed in the sample and not settling over time.

To determine if the amount of material in the solution controlled the thickness of the array, two arrays were made: one with the usual amount of coated quantum dots, and the other with only quantum dots (1 mL) and deionized water (1 mL) to dilute the solution in half. The results of this test should yield two identical arrays with the thickness of one half that of the other.

**Stöber nanoparticles.** Tetraethoxysilane (TEOS) (2.86 g) was stirred vigorously with methanol (100 mL) for five minutes before slowly adding concentrated ammonium hydroxide (7.2 mL). This reaction was stirred vigorously and reacted for 1 to 24 hours.[12,13]

## References


1. A. Wang, S.-L. Chen, and P. Dong, *Mater. Lett.*, 2009, **63**, 1586.
2. U. Jonas and C. Krüger, *J. Supramol. Chem.,* 2002, **2**, 255.
3. D. Mei, H. Liu, B. Cheng, Z. Li, and D. Zhang, *Phys. Rev. B,* 1998, **58**, 35.
4. R. Mayoral, J. Requena, J. Moya, C. Lopez, A. Cintas, H. Miguez, F. Meseguer, L. Vazquez, M. Holgado, and A. Blanco, *Adv. Mater.,* 1997, **9**, 257.
5. W. Wen, N. Wang, H. Ma, Z. Lin, W. Y. Tam, C. T. Chan, and P. Sheng, *Phys. Rev. Lett.,* 1999, **82**, 4248.
6. M. Cortalezzi, V. Colvin, and M. Wiesner, *J. Colloid Interf. Sci.,* 2005, **283**, 366.
7. Y. Min, M. Akbulut, K. Kristiansen, Y. Golan, and J. Israelachvil, *Nat. Mater.,* 2008, **7**, 527.
8. F. Piret, and B.-L. Su, *Chem. Phys. Lett.*, 2008, **457**, 376.
9. T. H. Kim, H. J. Kim, T. S. Lee, and W. S. Lyoo, *Mol. Cryst. Liq. Cryst.,* 2007, **464**, 153.
10. J. Yang; unpublished results.
11. H.-L. Li and F. Marlow, *Chem. Mater.*, 2006, **18**, 1803.
12. W. Stöber, A. Fink, and E. Bohn, *J. Colloid Interf. Sci.,* 1968, **26**, 62.
13. M. Litschauer and M.-A. Neouze, *J. Mater. Chem.*, 2008, **18**, 640.

# Conclusions

Both the silicon and germanium quantum dots were successfully synthesized and made hydrophilic. Coating these quantum dots with silica, with an LPD method, to yield only a 10 nm separation between them proved to be a more challenging task, but coating these particles in the presence of DTAB as a surfactant and allowing the reaction to go for only 6 hours yielded the desired silica coating. The silica coating was found to be successful for particles which have electronegative capping ligands. These particles were then organized in an array by a vertical deposition method using deionized water as the solvent, and the array was nearly close packed. The thickness of the array could be controlled with the concentration of the particles in the solution for the coated Si QDs, but the coated Ge QDs did not array below the high concentration. The arrays were tested for photoconductivity, and although the results were inconsistent, the cells were proven to be conductive in areas. With further improvement, these cells could be conductive across the board.

# Publications and Presentations

"Synthesis and characterization of dielectric coated Si and Ge quantum dots" SE/SW Regional American Chemical Society presentation, New Orleans, LA 2010

"Thin Films of Silica Imbedded Silicon and Germanium Quantum Dots by Solution Processing" Submitted to *Mat. Sci. Semicon. Proc.*